Faculty of Natural Science and Technology
Department of Physics

NTNU
Innovation and Creativity

MASTER'S THESIS FOR

STUD. TECHN. HALVOR LUND

Thesis started:	26.01.2009
Thesis submitted:	19.06.2009

DISCIPLINE: THEORETICAL PHYSICS

Norsk tittel: *"Epidemi-spredning på komplekse nettverk: En reaksjon-diffusjon-tilnærming"*

English title: *"Epidemic Spreading on Complex Networks: A Reaction-Diffusion Approach"*

This work has been carried out at Department of Physics, under the supervision of Prof. Ingve Simonsen.

Trondheim, 19.06.2009

Ingve Simonsen

Responsible supervisor

Professor at Department of Physics

Preface

This master's thesis was written during the spring of 2009 as the final part of my Master of Science degree in Applied Physics and Mathematics at NTNU, with specialization in Technical Physics.

Working with the thesis has been both interesting, rewarding and sometimes fun. I have learned a lot about the world of scientific research, and I was happy to discover that I actually could contribute to it.

I would like to thank my supervisor, Ingve Simonsen, for his invaluable advice and always positive attitude. Thanks also to Henrik Enoksen for proofreading and useful discussions. Finally, thanks to my dear Rikke for always encouraging me and cheering me up.

Halvor Lund
Trondheim, June 2009

Abstract

An epidemic spreading model known as the SIS (Susceptible-Infected-Susceptible) model with diffusion on complex networks is studied, with emphasis on the long-term behavior (the stationary state) of the number of infected particles. Both analytical (mean-field) and simulation results for both discrete and continuous time are presented. This model has been studied previously by Colizza *et al.* (Nat. Phys. 3:276-282, 2007). They found that the model has a phase transition at a critical density, which is dependent on network topology. Our simulation results show that the analytical results presented by Colizza *et al.* are correct. We suggest that their simulations deviate from the analytical results because of excessively high reaction rates. The analytical results for the stationary state are generalized using a series expansion in the node degree k, which agrees with simulation results. A new and presumably more realistic reaction type is also introduced. The critical density's dependence on diffusion and reaction rates is calculated both analytically (using a series expansion and a Jacobian matrix) and by simulation, and these coincide. Finally, we present a model for opinion formation and spreading on a complex network, which shows some interesting behavior.

Sammendrag

Vi undersøker en modell for epidemi-spredning kjent som SIS-modellen (Susceptible-Infected-Susceptible) med diffusjon på komplekse nettverk, med fokus på den langsiktige oppførselen (den stasjonære tilstanden) til antallet infiserte partikler. Både analytiske (middelfelt) og simuleringsresultater med både diskret og kontinuerlig tid blir presentert. Denne modellen har blitt studert tidligere av Colizza *et al.* (Nat. Phys. 3:276-282, 2007). De fant at modellen har en faseovergang ved en kritisk tetthet som er avhengig av nettverksstrukturen. Våre simuleringsresultater viser at de analytiske resultatene som Colizza *et al.* presenterte er riktige. Vi antyder at deres simuleringer avviker fra de analytiske uttrykkene på grunn av for høye reaksjonshastigheter. De analytiske resultatene for stasjonærtilstanden blir generalisert ved å rekkeutvikle i node-rangen k, og disse resultatene stemmer med simuleringer. Vi introduserer også en ny og formodentlig mer realistisk reaksjonstype. Den kritiske tetthetens avhengighet av diffusjons- og reaksjonshastighetene blir beregnet både analytisk (med rekkeutvikling og Jacobi-matrise) og ved simulering, og disse stemmer overens. Til slutt presenterer vi en modell for meningsdannelse og -spredning på komplekse nettverk, som viser seg å ha en interessant oppførsel.

Contents

Chapter 1

Introduction

We live in a complex world. Although we have a good understanding of the smallest constituents of the universe, like protons and electrons, a thorough understanding of more intricate systems may be harder to obtain. Our understanding of elementary particles is of little use when we for instance try to understand the working principles of a group of people, which is composed of billions upon billions of electrons and protons. To deal with such intricate systems or networks, we need some kind of simplification.

So what is a network? Simply speaking, a network consists of objects with some connections between them. In many contexts, "network" will be synonymous with "system". In the real world, you can find numerous examples of networks or systems. You, your friends and your friends' friends make up a network of friendships, relationships and acquaintances. The web pages in the World Wide Web and their hyperlinks make up a network, while the routers of the Internet and their communcation make up another. None of these are easy to fully understand: There is more to a system than just the sum of its parts, just as a network is more complex than a collection of individual objects. Or, as expressed by Craig Reynolds, "a flock is not a big bird" [1]. The interactions between the objects make networks both interesting and challenging.

Already in the 1930s, social networks were studied extensively by sociologists. They discovered how important the structure of such networks was to their function. The way friends interact, for example, would have a great effect on how a rumour or a disease would spread between them. If you were sick and met lots of friends every day, you would naturally expose more people to the disease than if you had no friends and never left your home. An obstacle in the study of social networks, however, was to obtain reliable data about these networks.

When computers and more extensive network data became available later in the 20th century, the study of networks took a new turn. Instead of studying just small networks, one could now consider networks with thousands or even millions of objects. Computer networks, such as the Internet, was studied, and one realized how the structure could have an impact on the spread of computer viruses or the vulnerability to targeted attacks.

One of the important applications of the study of networks is what's known as *epidemic*

modeling. This concerns the way a disease, a virus or something similar spreads in a network. As mentioned previously, the way in which people or computers interact is clearly crucial to such spreading.

The goal of this project was to study a type of epidemic modeling on networks that resemble those found in the real world. Previously work has already been done to find the long-term limit (stationary state) in such systems. The stationary state can give useful information about whether an infection will spread or die out. I intend to investigate these results in more detail and try to generalize and compare them. I will also present a model for opinion formation and spreading on networks, which in principle is quite similar to the epidemic model.

Chapter 2

Theory

The following theory section, giving an introduction to modeling of networks and reaction-diffusion, is largely taken from my project thesis [2].

To study the properties of real networks, we need to make a model to represent their most important properties. As mentioned in the introduction, a network consists of objects with some connections. To incorporate these two elements, we use what is known in mathematics as a *graph*.

In a graph, the objects are called nodes or vertices, while the connections between them are called links or edges. The links may be directed, which means that a link from node u to node v does not necessarily imply a link from v to u. Undirected links, on the other hand, can be traversed in both directions. Links may also have a weight assigned to them, in order to indicate *e.g.* the cost of using each link or the link's capacity. In graph theory, the word "network" is used for directed, weighted graphs, but we will use it as a synonym for a graph. An example of a small, undirected, unweighted network is given in Fig. 2.1.

Each node has a *degree*, k, defined as its number of connections to other nodes. In Fig. 2.1, the degrees vary from 1 to 4. The degree distribution, $p(k)$, is important for the network's properties. Large variations in the nodes' degrees contributes to the complexity that a network often has. Although the mean degree $\langle k \rangle$ is low, the maximum degree $k_{\max}$ can be quite high. Real-world networks are often heterogeneous, *i.e.* they have large degree variations. This as opposed to a homogeneous system with nodes in a regular lattice, with only links to nearest neighbors. For instance, in a regular square 2D lattice, all nodes not on the edges have degree 4, and in this respect they are equivalent, hence the network is homogeneous.

Another often used quantity is the *shortest path* between two nodes, or *geodesic path*. The geodesic path between two nodes is the shortest distance between them by traversing the network. In a network where all links have a unit weight, the shortest path length is equal to the lowest number of links you have to use to travel from one node to the other. An important property of many networks is that the average distance between nodes increases slowly when increasing the number of nodes. This is known as the *small-world effect*. Networks are said to show the small-world effect if the average distance between

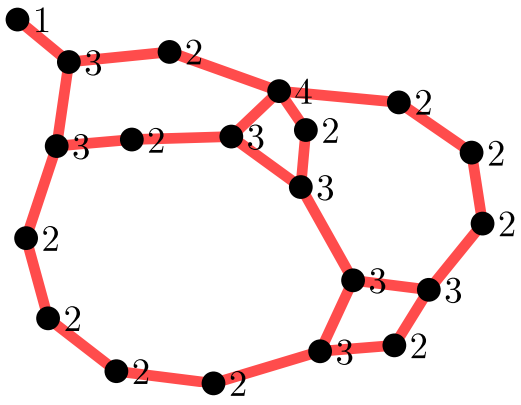

Figure 2.1: An example of a network with 20 nodes. The number next to each node is its degree k.

two nodes scales logarithmically, or slower, for a fixed mean degree $\langle k \rangle$.

2.1 Types of networks

2.1.1 Erdös-Rényi networks

Erdös and Rényi [3] proposed a simple model for networks, which shows the important small-world effect. The model takes a number of vertices V and connects each pair with a probability p. In other words, each possible link between two nodes is equally probable. These networks have a binomial distribution of degrees, which approaches a Poisson distribution when $n \to \infty$ holding the mean degree $\langle k \rangle = p(V-1)$ constant. Therefore, these networks or graphs are also known as Poisson random graphs. Although this model shows the small-world effect, an important property of real networks, the degree distribution is not similar to that of most real networks.

2.1.2 Scale-free networks

A large variety of real networks have shown to be *scale-free*. More precisely, the degree distribution scales as $p(k) \sim k^{-\gamma}$ where $\gamma > 0$ is some exponent, or in other words $p(k)$ is a power law. Two degree distributions of real networks are shown in Fig. 2.2. A summary of this and other properties of different real networks can be found in *e.g.* recent reviews by Albert and Barabási [4] or Newman [5].

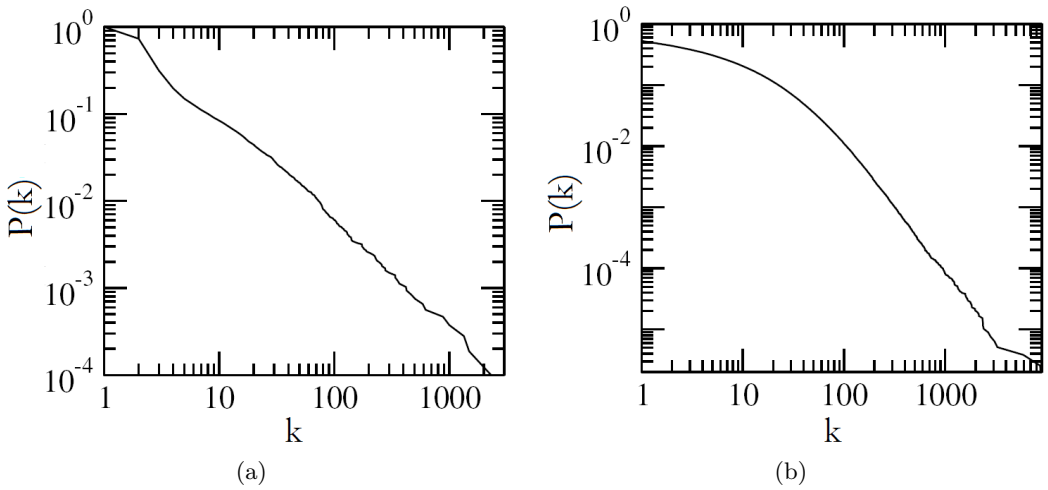

Figure 2.2: Cumulative degree distributions of (a) the Internet (γ = 2.5) [6] and (b) a scientific citation network (γ = 3.0) [7]. (Figure by Newman [5])

2.2 Reaction-diffusion

A network may be used as a model for a real system in which particles interact. These particles may be network packages exchanged between computers in a computer network, a rumour spreading in a friendship network *etc.* The transportation and reactions of these particles may be quite interesting in the complex networks that you often find in real life. In *epidemic modeling*, a network is used to model the spread of a disease. People are modeled as two types of particles: susceptible (S) or infected/infectious (I). This is also known as the SIS model. One may also include a third type, recovered/resistent (R), which makes a SIR model. A SIS model will be studied in this thesis.

In a reaction-diffusion (RD) process on a complex network, particles *react at* and *diffuse between* the nodes. In this thesis, the studied reactions are

$$A + B \to 2B\,, \tag{2.1a}$$

$$B \to A\,. \tag{2.1b}$$

Interpreted in an epidemic scenario, the A particles are un-infected or susceptible, while B particles are infected/infectious. The first reaction (2.1a) represents the infection of susceptible particles, while the second reaction (2.1b) represents the recovery ("healing") of infected particles. In other words, reaction (2.1a) will *decrease* the number of A particles while reaction (2.1b) will *increase* the number of A particles. These equations also ensure that the total number of particles on the network is conserved at all times.

The starting point for this project was an article by Colizza *et al.* [8], where the reactions (2.1) were studied. These authors presented analytical expressions for the stationary state of such a system, and experimental (simulation) results were used to confirm these.

The results showed that there exists a phase transition at a critical total particle density. Below this critical density, the number of B particles vanishes with time, and becomes zero for the stationary state.

Colizza *et al.* [8] introduces two types of reactions for equation (2.1a). The first, type I, lets each B at a given node interact with all A's at that node, each interaction having a probability β for a reaction to take place. In a type II reaction, each B is only interacting with a limited number of A's. Colizza *et al.* found the two types (not surprisingly) to give rise to different behaviour, where type I reactions are the ones affected by network structure. Equation (2.1b) is modeled by letting each B be converted to an A with a probability μ.

If one let the nodes represent cities and particles represent people, the two reaction types can be interpreted as different social contexts. Type I reactions can be viewed as a case where "everyone knows everyone", as in a small town. Type II reactions may be a case where each person only interacts with a limited number of other people, not the whole city. This inspires us to define a new reaction type, type M (mixed), which is a combination of the two. Type M will (below) be defined to be similar to type I for small particle densities, that is "everyone knows everyone" in small towns. For large particle densities, type M is similar to type II, which limits the number of interactions. In this way, type M models the way in which people interact on both small and large city scales. Type M reactions are introduced for the first time in this thesis, and was not discussed in my project thesis [2].

Let $N_A(i,t)$ and $N_B(i,t)$ denote the number of particles of type A and B, respectively, at node i at time t. Instead of having an integer number of A and B particles, we let $N_A(i,t)$ and $N_B(i,t)$ be continuous. This may be viewed as letting the number of particles be (virtually) infinite. Since the total number of particles is conserved, it is implied that $\partial_t N_A(i,t) = -\partial_t N_B(i,t)$ with $i = 1, 2, ..., V$, where ∂_t is the time derivative.

If the first reaction, (2.1a), is type I, the number of possible interactions between A and B particles is $N_A(i,t)N_B(i,t)$, and each interaction ends in a reaction with probability β. Thus $\partial_t N_A(i,t) = -\beta N_A(i,t)N_B(i,t)$ for type I reactions. If the first reaction is type II, the number of interactions is rescaled with a factor $1/N(i,t)$, where $N(i,t) = N_A(i,t) + N_B(i,t)$ is the total number of particles at node i at time t. Thus $\partial_t N_A(i,t) = -\beta N_A(i,t)N_B(i,t)/N(i,t)$ for type II reactions. In the second reaction, (2.1b), each B turns into an A with probability μ, and thus $\partial_t N_A(i,t) = \mu N_B(i,t)$. Together, the two reactions (2.1) give rise to the following equation for $N_A(i,t)$ and $N_B(i,t)$:

$$\partial_t N_A(i,t) = -\partial_t N_B(i,t) = \mu N_B(i,t) - \beta N_A(i,t)N_B(i,t), \tag{2.2}$$

for type I reactions and

$$\partial_t N_A(i,t) = -\partial_t N_B(i,t) = \mu N_B(i,t) - \beta \frac{N_A(i,t)N_B(i,t)}{N(i,t)}, \tag{2.3}$$

for type II reactions.

Type M reactions are defined as

$$\partial_t N_A(i,t) = -\partial_t N_B(i,t) = \mu N_B(i,t) - \beta \frac{N_A(i,t) N_B(i,t)}{N_\times + N(i,t)}, \tag{2.4}$$

where $N_\times$ is a crossover density which describes the transition between type I and II. For $N(i,t) \ll N_\times$, we see that type M is approximately equal to type I (apart from a factor $1/N_\times$). For $N(i,t) \gg N_\times$, type M is approximately equal to type II.

These equations do not include the effects of diffusion, which redistributes the particles between the nodes and obviously is necessary for the complex behaviour of reaction-diffusion on networks. The diffusion process is implemented by letting each particle move to a neighboring node using one of the links. The probability of using a given link is $\frac{1}{k}$ where k is the degree of the present node (in an unweighted network). In this way, all links are equally probable. By specifying diffusion constants D_A and D_B for A and B particles respectively, one can adjust the probability that a particle will diffuse. $D_A = 1$ implies that all A particles diffuse, $D_A = 0$ implies no diffusion of A particles, and values in between indicates that only a fraction of the A particles diffuse.

Chapter 3

Implementation

This chapter is largely taken from my project thesis [2], but updated with new knowledge and changes. It describes some of the details of implementing and generating networks (or graphs, rather) and implementing reaction-diffusion.

3.1 Creating networks

To create a network given a certain degree distribution, we use the Molloy-Reed algorithm [9], shown in algorithm 1. This algorithm creates random links between the nodes according to the node degrees k_i, where k_i is the degree of node i. There are restrictions as to what degree distributions are possible, which are discussed in [9]. It works by making a list of nodes where each node i is listed k_i times, and then removing two random nodes from the list and making a link between them. In this way, each node i is connected to other nodes k_i times, thus getting a degree k_i.

The network with its links is stored in an *adjacency matrix* $\mathbf{A}$, which specifies which nodes are adjacent to each other, *i.e.* are connected by a link. It is defined so that $A_{ij} = 1$ if there is a link from j to i, zero otherwise. In this thesis, all links are un-directed, *i.e.* $A_{ij} = A_{ji}$ and the adjacency matrix is therefore symmetric in this case. As the mean degree $\langle k \rangle$ of a node in the scale-free networks is far lower than the number of nodes V, $\langle k \rangle \ll V$, this matrix is preferably stored as a sparse matrix.

In this thesis, most networks are scale-free. For a network with V nodes, we let the node degrees k satisfy $2 \leq k < \sqrt{V}$, which is the same restriction as Colizza *et al.* [8] have used. Each node is then simply given a degree k with probability $p(k) \sim k^{-\gamma}$. $p(k)$ is normalized so that $\sum_{k=2}^{\sqrt{V}} p(k) = 1$.

3.2 Reaction-diffusion

Colizza *et al.* [8] implemented the reaction-diffusion process as a *sequential process*. For each time step, they perform first a reaction step at each individual node, then diffusion

Algorithm 1: Molloy-Reed algorithm to generate networks with given degree sequence

```
Data: node degrees k_i
Result: links
create list V with k_i copies of node i for every node;
while V is not empty do
    pick two random nodes u and v from V;
    if no link between u and v then
        make link between u and v;
        remove u and v from V;
    end
end
```

between the nodes. They also have a discrete number of particles and simulate the reaction-diffusion stochastically with the Monte-Carlo algorithm. This implementation is presented in algorithm 4. To be able to compare our results with those of Colizza *et al.*, one of our implementations was identical to theirs.

Our main implementation, however, was a discrete time simulation. The differential equations were discretized with a forward difference scheme, by letting $\partial_t N_A(i,t) = N_A(i,t+1) - N_A(i,t)$ and $\partial_t N_B(i,t) = N_B(i,t+1) - N_B(i,t)$. The particle numbers $N_A(i,t)$ and $N_B(i,t)$ were continuous numbers, contrary to Colizza's integer particle numbers. The advantage with this implementation is that it is far less computationally demanding and gives more accurate results than the stochastic implementation.

We implemented the process both as a sequential and as a simultaneous process, with reaction and diffusion occuring simultaneously. As recently pointed out by Saldaña [10], the equations resulting from the sequential implementation does not have a well-defined continuous-time limit. Therefore a simultaneous implentation was also made. These two approaches are not equivalent in general, and the differences between the two approaches will be discussed in chapter 4. In total, one can combine this to four implementations, as shown in Table 3.1.

Table 3.1: Implementations of reaction-diffusion

	Simultaneous	**Sequential**
Stochastic	Not implemented	Colizza & Lund
Deterministic/Discretized diff. eq.	Lund	Lund

The reactions (2.1) are implemented by using Eq. (2.2) (type I), Eq. (2.3) (type II) or Eq. (2.4) (type M). The diffusion process was implemented using a *transfer matrix* $\mathbf{T}$, which "transfers" diffusing particles to neighboring nodes. $\mathbf{T}$ is based on the adjacency matrix $\mathbf{A}$, and its elements are given by $T_{ij} = \frac{A_{ij}}{\sum_i A_{ij}}$ [11]. This will give each link from a given node j the probability $\frac{1}{k_j}$, since $\sum_i A_{ij} = k_j$. We let $\boldsymbol{N_A}(t)$ be a column vector,

$$\boldsymbol{N_A}(t) = \begin{pmatrix} N_A(1,t) \\ N_A(2,t) \\ \vdots \\ N_A(V,t) \end{pmatrix}, \tag{3.1}$$

where $N_A(i,t)$, we recall, is the number of A particles at node i at time t, and similarly for $\boldsymbol{N_B}(t)$. We can then perform a diffusion step by calculating the matrix products

$$\boldsymbol{N_A}(t+1) = \mathbf{T}\boldsymbol{N_A}(t), \tag{3.2a}$$
$$\boldsymbol{N_B}(t+1) = \mathbf{T}\boldsymbol{N_B}(t). \tag{3.2b}$$

With discretized differential equations, the whole process, for type I reactions and sequential reaction and diffusion, was implemented as shown in algorithm 2, and similarly for type II and M reactions. Algorithm 3 shows the implementation for type I reactions and simultaneous reaction and diffusion. Finally, algorithm 4 shows the stochastic implementation as done by Colizza *et al.* [8] (and replicated by us), for type I reactions.

Algorithm 2: Implementation of the SIS model with diffusion on a network, type I, sequential/discrete-time

Data: $\mathbf{T}$, $\boldsymbol{N_A}(0)$, $\boldsymbol{N_B}(0)$, t_{end}
Result: $\boldsymbol{N_A}(t_{\text{end}})$, $\boldsymbol{N_B}(t_{\text{end}})$
$t = 0$;
while $t < t_{end}$ **do**
  $t = t + 1$;
  Reaction:
  $\boldsymbol{\Delta A} = \mu \boldsymbol{N_B}(t-1) - \beta \boldsymbol{N_A}(t-1)\boldsymbol{N_B}(t-1)$;
  $\boldsymbol{N_A}(t) = \boldsymbol{N_A}(t-1) + \boldsymbol{\Delta A}$;
  $\boldsymbol{N_B}(t) = \boldsymbol{N_B}(t-1) - \boldsymbol{\Delta A}$;
  Diffusion:
  $\boldsymbol{N_A}(t) = D_A \mathbf{T}\boldsymbol{N_A}(t) + (1 - D_A)\boldsymbol{N_A}(t)$;
  $\boldsymbol{N_B}(t) = D_B \mathbf{T}\boldsymbol{N_B}(t) + (1 - D_B)\boldsymbol{N_B}(t)$;
end

Algorithm 3: Implementation of the SIS model with diffusion on a network, type I, simultaneous/continuous-time

Data: $\mathbf{T}$, $\boldsymbol{N_A}(0)$, $\boldsymbol{N_B}(0)$, t_{end}
Result: $\boldsymbol{N_A}(t_{\text{end}})$, $\boldsymbol{N_B}(t_{\text{end}})$
$t = 0$;
while $t < t_{end}$ **do**
  $t = t + 1$;
  $\boldsymbol{N_A}(t) = (1-D_A)\boldsymbol{N_A}(t-1) + D_A\mathbf{T}\boldsymbol{N_A}(t-1) + \mu\boldsymbol{N_A}(t-1) - \beta\boldsymbol{N_A}(t-1)\boldsymbol{N_B}(t-1)$;
  $\boldsymbol{N_B}(t) = (1-D_B)\boldsymbol{N_B}(t-1) + D_B\mathbf{T}\boldsymbol{N_B}(t-1) - \mu\boldsymbol{N_A}(t-1) + \beta\boldsymbol{N_A}(t-1)\boldsymbol{N_B}(t-1)$;
end

Algorithm 4: Implementation of the SIS model with diffusion on a network, type I, sequential/discrete-time, stochastic

Data: $\mathbf{T}$, $\boldsymbol{N_A}(0)$, $\boldsymbol{N_B}(0)$, t_{end}
Result: $\boldsymbol{N_A}(t_{\text{end}})$, $\boldsymbol{N_B}(t_{\text{end}})$
$t = 0$;
while $t < t_{end}$ **do**
  $t = t + 1$;
  Reaction:
  foreach *node i in network* **do**
    foreach *of the $N_A(i,t)$ A particles* **do**
      React A+B → 2B with prob. $p_{A+B\to 2B} = (1 - (1-\beta)^{N_B(i,t)})$;
    end
    foreach *of the $N_B(i,t)$ B particles* **do**
      React B → A with prob. $p_{B\to A} = \mu$;
    end
  end
  Diffusion:
  foreach *node i in network* **do**
    foreach *of the $N_A(i,t)$ A particles* **do**
      Diffuse with prob. D_A with equal probability for each neighbor;
    end
    foreach *of the $N_B(i,t)$ B particles* **do**
      Diffuse with prob. D_B with equal probability for each neighbor;
    end
  end
end

Chapter 4

Results and discussion

We will now present both analytical and simulation results for the stationary state of the reaction-diffusion system. More specifically, we will look at the *nodal particle density* of B particles in the stationary state, *i.e.* the average number of B particles per node in the network.

As mentioned in the implementation section, Colizza *et al.* [8] implemented the reaction-diffusion process as a sequential process. Their analytical approach is based on this implementation, and as pointed out by Saldaña [10], the continuous-time limit of this two-step process is not well defined. This will be described in detail in the following chapter. Herein, we will present both the approach from Ref. [8], and a continuous-time approach (as suggested by Saldaña [10]).

Let $N_A(t)$ and $N_B(t)$ be the total number of A and B particles in the network at time t, respectively, and the total particle number we denote by $N = N_A(t) + N_B(t)$. The nodal density of particles, *i.e.* the average number of particles on each node, is defined as

$$\rho = \frac{N}{V} , \tag{4.1}$$

where V is the number of nodes in the underlying network. Colizza *et al.* use a mean-field approximation where all nodes with the same degree k are considered to be equivalent. Moreover, let $N_{A,k}$ and $N_{B,k}$ denote the total number of A and B particles, respectively, on nodes of degree k, V_k denote the number of nodes of degree k, and let

$$\rho_{A,k}(t) = \frac{N_{A,k}(t)}{V_k} , \tag{4.2a}$$

$$\rho_{B,k}(t) = \frac{N_{B,k}(t)}{V_k} , \tag{4.2b}$$

be the average number of A and B particles, respectively, on nodes of degree k. Similarly, one has

$$\rho_A(t) = \sum_k p(k)\rho_{A,k}(t) = \frac{N_A(t)}{V} \geq 0 \,, \tag{4.3a}$$

$$\rho_B(t) = \sum_k p(k)\rho_{B,k}(t) = \frac{N_B(t)}{V} \geq 0 \,, \tag{4.3b}$$

where $p(k)$ is the network's degree distribution, and $\rho = \rho_A(t) + \rho_B(t)$. Since the total number of particles in the network is conserved, ρ is constant in time.

4.1 Discrete-time reaction-diffusion

In the following subsection we will reproduce the discussion of Colizza *et al.* that was presented in their Nature Physics article [8]. As mentioned previously, they model the reaction-diffusion process with successive reaction and diffusion, as a process with two steps. Their equations for diffusion are

$$N_{A,k}(t+1) = N_{A,k}(t) - D_A N_{A,k}(t) + kV_k \sum_{k'} p(k'|k)\frac{D_A}{k'}\rho_{A,k'}(t) \,, \tag{4.4a}$$

$$N_{B,k}(t+1) = N_{B,k}(t) - D_B N_{B,k}(t) + kV_k \sum_{k'} p(k'|k)\frac{D_B}{k'}\rho_{B,k'}(t) \,, \tag{4.4b}$$

where $D_A,\ D_B \in [0,1]$ are the probabilities that an A or B particle, respectively, will diffuse. In a physical interpretation of Eq. (4.4), the first term is the number of particles already present at the node at time t, the second term is the diffusion of a fraction D_A or D_B of particles away from the nodes (of degree k), and the last term is the diffusion of particles into the nodes. $p(k'|k)$ in Eqs. (4.4) denotes the probability that a node of degree k' links to a node of degree k. If an uncorrelated network is assumed, then $p(k'|k) = p(k')k'/\langle k' \rangle$ [12]. Dividing Eq. (4.4) by V_k gives

$$\rho_{A,k}(t+1) = \rho_{A,k}(t) - D_A\rho_{A,k}(t) + \frac{D_A k}{\langle k \rangle}\sum_{k'} p(k')\rho_{A,k'}(t) \,, \tag{4.5a}$$

$$\rho_{B,k}(t+1) = \rho_{B,k}(t) - D_B\rho_{B,k}(t) + \frac{D_B k}{\langle k \rangle}\sum_{k'} p(k')\rho_{B,k'}(t) \,. \tag{4.5b}$$

Before each diffusion step, there is a reaction taking place at each node. This will change the ratio of A and B particles at each node. Based on Eq. (2.2), (2.3) and (2.4), the reaction at nodes of degree k gives the following equations:

$$N_{A,k}(t) = N_{A,k}(t-1) + \mu N_{B,k}(t-1) - V_k\beta\Gamma_k(t-1) \,,$$
$$N_{B,k}(t) = N_{B,k}(t-1) - \mu N_{B,k}(t-1) + V_k\beta\Gamma_k(t-1) \,,$$

or, divided by V_k:

$$\rho_{A,k}(t) = \rho_{A,k}(t-1) + \mu\rho_{B,k}(t-1) - \beta\Gamma_k(t-1) \,, \tag{4.6a}$$
$$\rho_{B,k}(t) = (1-\mu)\rho_{B,k}(t-1) + \beta\Gamma_k(t-1) \,, \tag{4.6b}$$

where Colizza *et al.* have introduced $\Gamma_k(t)$, the *reaction kernel*, which depends on the type of reaction. The average reaction kernel is denoted $\Gamma = \sum_k p(k)\Gamma_k$.

For the different reaction types that we will consider, the reaction kernel reads

$$\Gamma_k = \begin{cases} \rho_{A,k}\rho_{B,k} \,, & \text{for type I,} \\ \rho_{A,k}\rho_{B,k}/\rho_k \,, & \text{for type II,} \\ \rho_{A,k}\rho_{B,k}/(\rho_k + \rho_\times) \,, & \text{for type M.} \end{cases}$$

where $\rho_\times \equiv N_\times$. $N_\times$, we recall, is a density describing where type M goes from "type I-like" to "type II-like".

To combine reaction and diffusion (although this step is not apparent in Ref. [8]), we insert the right-hand sides from Eqs. (4.6) as $\rho_{A,k}(t)$ and $\rho_{B,k}(t)$, respectively, in Eqs. (4.5), to obtain

$$\begin{aligned} \rho_{A,k}(t+1) &= (1-D_A)\left[\rho_{A,k}(t-1) + \mu\rho_{B,k}(t-1) - \beta\Gamma_k(t-1)\right] \\ &\quad + \frac{D_A k}{\langle k\rangle}\sum_{k'} p(k')\left[\rho_{A,k'}(t-1) + \mu\rho_{B,k'}(t-1) - \beta\Gamma_{k'}(t-1)\right] \,, \end{aligned} \tag{4.7a}$$
$$\begin{aligned} \rho_{B,k}(t+1) &= (1-D_B)\left[(1-\mu)\rho_{B,k}(t-1) + \beta\Gamma_k(t-1)\right] \\ &\quad + \frac{D_B k}{\langle k\rangle}\sum_{k'} p(k')\left[(1-\mu)\rho_{B,k'}(t-1) + \beta\Gamma_{k'}(t-1)\right] \,. \end{aligned} \tag{4.7b}$$

We now transform equations (4.7) to a coupled set of differential equations and do the summation over k', to get

$$\begin{aligned} \partial_t\rho_{A,k}(t) &= -\rho_{A,k}(t) + (1-D_A)\left[\rho_{A,k}(t) + \mu\rho_{B,k}(t) - \beta\Gamma_k(t)\right] \\ &\quad + \frac{D_A k}{\langle k\rangle}\left[\rho_A(t) + \mu\rho_B(t) - \beta\Gamma(t)\right] \,, \end{aligned} \tag{4.8a}$$
$$\begin{aligned} \partial_t\rho_{B,k}(t) &= -\rho_{B,k}(t) + (1-D_B)\left[(1-\mu)\rho_{B,k}(t) + \beta\Gamma_k(t)\right] \\ &\quad + \frac{D_B k}{\langle k\rangle}\left[(1-\mu)\rho_B(t) + \beta\Gamma(t)\right] \,, \end{aligned} \tag{4.8b}$$

which are the equations presented in the supplementary information to Ref. [8]. In this transformation, Colizza *et al.* apparently let $\partial_t\rho_{A,k} = \rho_{A,k}(t+2) - \rho_{A,k}(t)$ (and similar for $\rho_{B,k}$), which is not in agreement with the ordinary definition of a derivative: $\partial_x f(x) = \lim_{h\to 0}\frac{f(x+h)-f(x)}{h}$. This is the crucial point where the approach of Colizza *et al.* deviates

from the approach suggested by Saldaña [10]. The differences will be discussed in further detail in section 4.2.

We now want to find the stationary state of these equations, *i.e.* where the solutions satisfy $\partial_t \rho_{B,k} = \partial_t \rho_{A,k} = 0$. A trivial solution is $\rho_B = 0$ and $\rho_A = \rho$, but this is of little interest to us here. To find a nontrivial solution, we use Eqs. (4.8) and get

$$\overline{\rho}_{A,k} = (1 - D_A)\left[\overline{\rho}_{A,k} + \mu\overline{\rho}_{B,k} - \beta\overline{\Gamma}_k\right] + \frac{D_A k}{\langle k\rangle}\left[\overline{\rho}_A + \mu\overline{\rho}_B - \beta\overline{\Gamma}\right] , \tag{4.9a}$$

$$\overline{\rho}_{B,k} = (1 - D_B)\left[(1-\mu)\overline{\rho}_{B,k} + \beta\overline{\Gamma}_k\right] + \frac{D_B k}{\langle k\rangle}\left[(1-\mu)\overline{\rho}_B + \beta\overline{\Gamma}\right] , \tag{4.9b}$$

where barred symbols (*e.g.* $\overline{\rho}_{A,k}$) indicate the stationary state of each quantity. Colizza *et al.* [8] then multiply equation (4.9a) by $p(k)$ and sum over k to obtain

$$\overline{\rho}_B = \frac{\beta}{\mu}\overline{\Gamma}. \tag{4.10}$$

Equations (4.9) are then simplified to

$$\overline{\rho}_{A,k} = (1 - D_A)\left[\overline{\rho}_{A,k} + \mu\overline{\rho}_{B,k} - \beta\overline{\Gamma}_k\right] + \frac{D_A k}{\langle k\rangle}\overline{\rho}_A, \tag{4.11a}$$

$$\overline{\rho}_{B,k} = (1 - D_B)\left[(1-\mu)\overline{\rho}_{B,k} + \beta\overline{\Gamma}_k\right] + \frac{D_B k}{\langle k\rangle}\overline{\rho}_B . \tag{4.11b}$$

These equations are presented in Ref. [8]. Solving explicitly for $\overline{\rho}_{A,k}$ and $\overline{\rho}_{B,k}$ is done by Colizza *et al.* for the cases when $D_B = 1$ and $D_A \in \{0, 1\}$, and we will reproduce their findings below for these special cases.

4.1.1 Special cases: $D_B = 1$ and $D_A \in \{0, 1\}$

The following results for type I and II are mainly based on my project thesis [2], which in turn are similar to the calculations in the supplementary information to Ref. [8]. The results for the introduced type M, however, are new in this thesis.

Case 1: Non-diffusing A particles ($D_A = 0$, $D_B = 1$)

In this case, the general result (valid for all reaction types) is given by equation (4.11a), which yields

$$\overline{\rho}_{B,k} = \frac{\beta}{\mu}\overline{\Gamma}_k . \tag{4.12}$$

From equation (4.11b) we also find that

$$\overline{\rho}_{B,k} = \frac{k}{\langle k\rangle}\overline{\rho}_B \tag{4.13}$$

in this case. The diffusion of B particles thus leads to the density $\overline{\rho}_{B,k}$ being proportional to the node degree k, which would also be the case with only diffusion [11].

- For type I reactions, we use equation (4.12) and the definition of the reaction kernel, $\Gamma_k = \rho_{A,k}\rho_{B,k}$, and get

$$\overline{\rho}_A = \overline{\rho}_{A,k} = \frac{\mu}{\beta}, \tag{4.14a}$$

$$\overline{\rho}_B = \rho - \frac{\mu}{\beta}. \tag{4.14b}$$

  Since $\overline{\rho}_B \geq 0$, these equations only apply when $\rho \geq \mu/\beta$. Below this critical value, $\overline{\rho}_B = 0$, and above it, $\overline{\rho}_B > 0$. We therefore have a *phase transition* at the critical density

$$\rho_c = \frac{\mu}{\beta}\,.$$

  We can also note that the density of A particles is independent of degree, *i.e.* there is an equal number of A particles on every node.

- For type II reactions, equation (4.12) and $\Gamma_k = \rho_{A,k}\rho_{B,k}/\rho_k$ gives us

$$\overline{\rho}_{A,k} = \frac{\beta}{\mu}(\overline{\rho}_{A,k} + \overline{\rho}_{B,k})\,. \tag{4.15}$$

  Multiplying by $p(k)$ and summing over k yields the stationary densities

$$\overline{\rho}_A = \frac{\mu}{\beta}\rho\,, \tag{4.16a}$$

$$\overline{\rho}_B = \rho\left(1 - \frac{\mu}{\beta}\right)\,. \tag{4.16b}$$

  In this case, we have a phase transition when varying μ/β, and the transition occurs at $\mu/\beta = 1$. For $\mu/\beta > 1$, $\overline{\rho}_B = 0$, and when $\mu/\beta < 1$, $\overline{\rho}_B$ is non-vanishing.

  To find an expression for $\overline{\rho}_{A,k}$, we insert the expression for $\overline{\rho}_{B,k}$ from Eq. (4.13) into Eq. (4.15) to get

$$\overline{\rho}_{A,k} = \frac{k}{\langle k\rangle}\frac{\mu}{\beta}\rho\,.$$

  Surprisingly, even without diffusion, the A particle density is linearly dependent on the degree k. This dependence can only be a result of the diffusion of B particles, since only diffusion depends on the nodes' degrees.

- For type M reactions, equation (4.12) and $\Gamma_k = \rho_{A,k}\rho_{B,k}/(\rho_\times + \rho_k)$ gives us

$$\overline{\rho}_{B,k} = \frac{\beta}{\mu}\frac{\overline{\rho}_{A,k}\overline{\rho}_{B,k}}{\rho_\times + \overline{\rho}_{A,k} + \overline{\rho}_{B,k}} \, .$$

  Dividing by $\overline{\rho}_{B,k}$ and multiplying by the divisor yields

$$\rho_\times + \overline{\rho}_{A,k} + \overline{\rho}_{B,k} = \frac{\beta}{\mu}\overline{\rho}_{A,k} \, . \tag{4.17}$$

  By multiplying by the degree distribution $p(k)$ and summing over k, we obtain an expression for $\overline{\rho}_A$:

$$\begin{aligned} \overline{\rho}_A &= \frac{\mu}{\beta}(\rho_\times + \rho) \, , \\ \overline{\rho}_B &= \rho\left(1 - \frac{\mu}{\beta}\right) - \frac{\mu}{\beta}\rho_\times \, . \end{aligned} \tag{4.18}$$

  The phase transition in this case occurs at the critical density

$$\rho_c = \frac{\mu}{\beta - \mu}\rho_\times \, ,$$

  and $\overline{\rho}_B$ is non-vanishing whenever $\rho > \rho_c$. If we let $\rho_\times \to 0$, we retrieve the results we got for type II, as expected. When $\rho_\times \to \infty$, while holding $\rho_\times/\beta$ constant, the results are equal to those for type I, apart from the factor $\rho_\times$.

Case 2: Diffusing A particles ($D_A = 1$, $D_B = 1$)

In this case, equations (4.11) give us a general result for all reaction types;

$$\overline{\rho}_{A,k} = \frac{k}{\langle k \rangle}\overline{\rho}_A \, , \tag{4.19a}$$

$$\overline{\rho}_{B,k} = \frac{k}{\langle k \rangle}\overline{\rho}_B \, . \tag{4.19b}$$

We see that the densities $\overline{\rho}_{A,k}$ and $\overline{\rho}_{B,k}$ are linear in k, which is also the case when having only diffusion on the network (without any reactions) [11].

- In the case of type I reactions, these two equations combined with Eq. (4.10) and the definition of Γ gives us $\overline{\rho}_B$:

$$\overline{\rho}_B = \frac{\beta}{\mu}\overline{\Gamma} = \frac{\beta}{\mu}\sum_k p(k)\overline{\rho}_{A,k}\overline{\rho}_{B,k} = \frac{\beta\langle k^2 \rangle}{\mu\langle k \rangle^2}\overline{\rho}_B\overline{\rho}_A$$

  Dividing by $\overline{\rho}_B$, we finally get

$$\overline{\rho}_A = \frac{\mu\langle k\rangle^2}{\beta\langle k^2\rangle} , \tag{4.20a}$$

$$\overline{\rho}_B = \rho - \frac{\mu\langle k\rangle^2}{\beta\langle k^2\rangle} . \tag{4.20b}$$

This time the phase transition occurs at the critical density

$$\rho_c = \frac{\mu\langle k\rangle^2}{\beta\langle k^2\rangle} .$$

The dependence on the mean degree and mean square degree means the phase transition is affected by the network topology. If we consider for example a regular 2D lattice, every node has 4 neighbours, *i.e.* a degree of 4, thus giving $\langle k\rangle^2 = \langle k^2\rangle = 16$. For a scale-free network, however, there is a considerable heterogeneity in the degrees, and the second moment $\langle k^2\rangle$ may be far larger than $\langle k\rangle^2$ (or even diverge). Thus, a scale-free network will have a lower critical density (for type I) and be more efficient at spreading an infection than a lattice.

- For type II reactions, we also use Eqs. (4.10) and (4.19) and get

$$\overline{\rho}_B = \frac{\beta}{\mu}\overline{\Gamma} = \frac{\beta}{\mu}\sum_k p(k)\frac{\overline{\rho}_{A,k}\overline{\rho}_{B,k}}{\overline{\rho}_k} = \frac{\beta}{\mu}\sum_k p(k)\frac{k\overline{\rho}_A\overline{\rho}_B}{\langle k\rangle\rho} = \frac{\beta}{\mu}\frac{\overline{\rho}_B\overline{\rho}_A}{\rho} .$$

Dividing by $\overline{\rho}_B$, we finally get

$$\overline{\rho}_A = \frac{\mu}{\beta}\rho , \tag{4.21a}$$

$$\overline{\rho}_B = \rho\left(1 - \frac{\mu}{\beta}\right) , \tag{4.21b}$$

which is the same as in the case with nondiffusing A particles. Since in both this case and the previous one, $\overline{\rho}_{A,k} = k/\langle k\rangle\overline{\rho}_A$, this result would be to expect.

- For type M reactions, Eqs. (4.10) and (4.19) give us

$$\overline{\rho}_B = \frac{\beta}{\mu}\sum_k p(k)\frac{\overline{\rho}_A\overline{\rho}_B\frac{k^2}{\langle k\rangle^2}}{\rho_\times + \rho\frac{k}{\langle k\rangle}} .$$

Rearranging this equation, using $\rho = \overline{\rho}_A + \overline{\rho}_B$, gives

$$\overline{\rho}_B = \rho - \frac{\mu}{\beta}\langle k\rangle\left(\sum_k p(k)\frac{k^2}{\langle k\rangle\rho_\times + k\rho}\right)^{-1} . \tag{4.22}$$

Although it is not possible to express $\overline{\rho}_B$ explicitly as a function of moments ($\langle k\rangle$, $\langle k^2\rangle$ etc.), the formula can be confirmed with simulations when having an actual degree distribution $p(k)$.

Summary

The results for the stationary states with $D_B = 1$ can be summarized as follows:

- For type I (as presented by Colizza *et al.* [8]), the stationary state is

$$\overline{\rho}_B = \begin{cases} \rho - \rho_c \,, & \text{if } \rho > \rho_c, \\ 0 \,, & \text{if } \rho \leq \rho_c, \end{cases}$$

  where the critical density is dependent on D_A;

$$\rho_c = \begin{cases} \frac{\mu}{\beta} \,, & \text{if } D_A = 0, \\ \frac{\mu \langle k \rangle^2}{\beta \langle k^2 \rangle} \,, & \text{if } D_A = 1. \end{cases}$$

- For type II (also presented by Colizza *et al.* [8]), the stationary state (for $D_A \in \{0, 1\}$) is

$$\overline{\rho}_B = \begin{cases} \rho \left(1 - \frac{\mu}{\beta}\right) \,, & \text{if } \mu < \beta, \\ 0 \,, & \text{if } \mu \geq \beta. \end{cases}$$

- For the new mixed type introduced by us, type M, the result for $D_A = 0$ is

$$\overline{\rho}_B = \begin{cases} \rho - \rho_c \,, & \text{if } \rho > \rho_c, \\ 0 \,, & \text{if } \rho \leq \rho_c, \end{cases}$$

  where the critical density is

$$\rho_c = \frac{\mu}{\beta - \mu} \rho_\times \,.$$

  For $D_A = 1$, the stationary state for type M is

$$\overline{\rho}_B = \max \left\{ 0, \rho - \frac{\mu}{\beta} \langle k \rangle \left(\sum_k p(k) \frac{k^2}{\langle k \rangle \rho_\times + k\rho} \right)^{-1} \right\} \,.$$

To better illustrate the differences between the stationary states of type I, II and M, we plot the above expressions in Fig. 4.1. The figure shows $\overline{\rho}_B / \rho = \overline{N}_B / N$, *i.e.* the fraction of B particles in the stationary state. The expressions are plotted both as functions of ρ (Fig. 4.1(a)) and β/μ (Fig. 4.1(b)). We observe that, for type I and M, non-diffusing A particles inhibits the infection and alters the phase transition, although the diffusion of the infected B particles is the same. This illustrates that diffusion is important for concentrating the A and B particles at high degree nodes, hence increasing the infection rate (*i.e.* the reaction kernel).

The existence of a phase transition means that there is an abrupt change in the long-term behaviour of the system at this transition. By changing only the total particle density ρ, one can get very different results. Below the phase transition, there will never be a long-term infectious state in the network. Above it, an infection can spread and persist with a non-zero fraction of B particles. This happens even though the equations for reaction and diffusion are exactly the same for the two regimes.

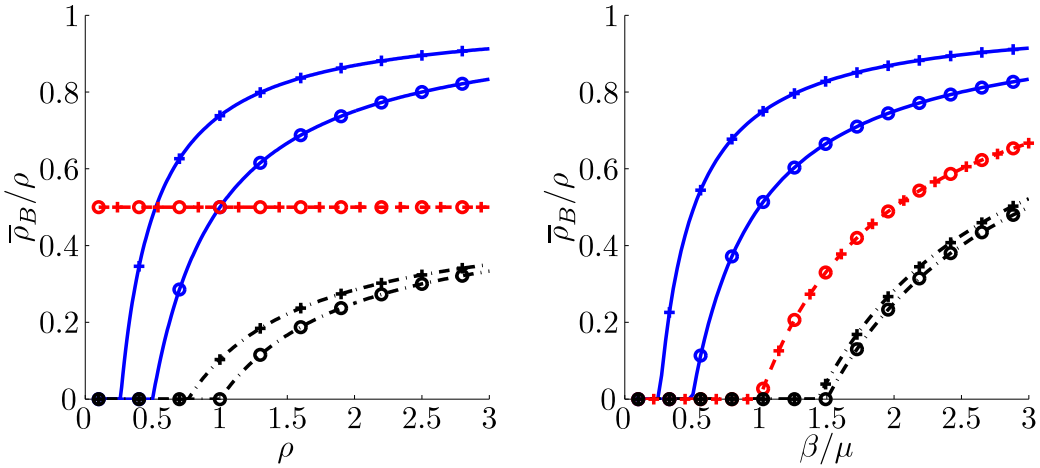

(a) $\beta/\mu = 2$ (b) $\rho = 2$

Figure 4.1: Analytical expressions for stationary states of type I, II and M ($\rho_\times = 1$) with diffusing B particles ($D_B = 1$), from Eqs. (4.14), (4.16), (4.18), (4.20), (4.21) and (4.22). Solid lines are type I, dashed lines are type II and dash-dot lines are type M. Circles indicate $D_A = 0$, cross (+) indicates $D_A = 1$. The network is scale-free with $V = 1000$ nodes and $\gamma = 2.5$.

Simulation results

We will now confront these mean-field analytical results with simulation results. In their Nature Physics paper [8], Colizza, Vespignani and Pastor-Satorras also present simulation results for the special cases presented above. In my project thesis [2], I performed similar simulations and compared the results. As mentioned in section 3.2, Colizza *et al.* implements the process stochastically, with integer particle number, while we implemented it with a forward difference of the differential equations. Since the two implementations are based on the same equations, the simulation results should be equal, apart from stochastical noise.

First we consider type I reactions. As mentioned earlier, there is a phase transition at the critical nodal particle density $\rho_c = \frac{\mu}{\beta}$ ($D_A = 0$) or $\rho_c = \frac{\mu}{\beta}\frac{\langle k\rangle^2}{\langle k^2\rangle}$ ($D_A = 1$). The simulation results presented by Colizza *et al.* [8] also show this important phase transition, with more or less accuracy. Their results together with those of my project thesis [2] are shown in Fig. 4.2. In this figure we plot $\overline{\rho}_B/\rho = \overline{N}_B/N$, *i.e.* the fraction of B particles in the stationary state.

As shown in Fig. 4.2(b), our simulation results closely match the analytical mean-field predictions, which should serve as a confirmation that our simulations are correct. For Colizza's results, however, it turns out that there are quite large deviations between the analytical predicitions and the simulation results (see Fig. 4.2(a)). The positions of the phase transitions are not accurate, and neither is the results for densities far from the the phase transition. For the largest network ($V = 10^5$), for example, the density of B particles

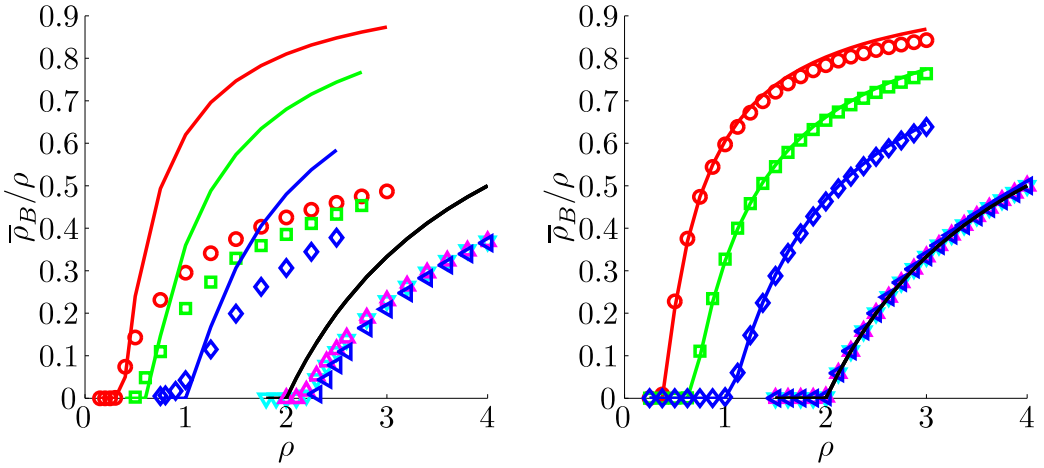

(a) Colizza (stochastic, μ and β unkown). Simulation results read directly from figure in Ref. [8], analytical results superimposed by us.

(b) Lund [2] (deterministic, $\mu = 0.02$, $\beta = 0.01$)

Figure 4.2: Comparison of (a) Colizza's [8] and (b) Lund's [2] simulation results for type I reactions, with $\mu/\beta = 2$ and $D_B = 1$. Lines indicate analytical results (Eqs. (4.14) and (4.20)), symbols are simulation results. Each symbol with properties (γ, V, D_A): Circles $\circ$ (2.5, 10^5, 1), squares $\square$ (2.5, 10^4, 1), diamonds $\diamond$ (2.5, 10^3, 1), downward triangle $\triangledown$ (2.5, 10^4, 0), upward triangle $\triangle$ (2.5, 10^5, 0), leftward triangle $\triangleleft$ (3.0, 10^4, 0).

$\overline{\rho}_B$ at $\rho = 3$ is only half of what the analytical expression predicts. The reason for these large differences was not found in my project thesis [2], but will be discussed below.

For type II reactions, the relative density of B particles, $\overline{\rho}_B/\rho$, is just dependent on β/μ, not on ρ. In this case, the phase transition occurs when $\beta/\mu = 1$. Colizza *et al.* [8] therefore present a simulation where they vary the ratio β/μ, as shown in Fig. 4.3(a). The results of my project thesis [2] are shown in Fig. 4.3(b). Again we observe the same picture, namely that Colizza's values are too low, and also here the phase transition is slightly off. Our results, however, are exactly on top of the analytical predictions.

As shown in Fig. 4.2 and Fig. 4.3, our simulation results was in very good agreement with the analytical mean-field predictions. However, the reason for Colizza's errors was not found in my project thesis [2]. As noted in section 3.2, Colizza *et al.* implemented the reaction-diffusion process stochastically, with integer particle number. We therefore tried performing simulations with the same implementation. For type I, rather high values of μ and β gave very similar results to those of Colizza, as shown in Fig. 4.4.

The results indicate that Colizza *et al.* have used too high values for the reaction coefficients μ and β, and that this is the reason why their results are not accurate. Too high values for μ and β will cause the reaction probability for each particle to exceed 1, something that is not self-consistent. This will lead to a "saturation" of the reaction, since a probability > 1 implies that a particle should participate in more than one reaction.

Fig. 4.4(c) shows results for lower reaction coefficients, which is significantly better

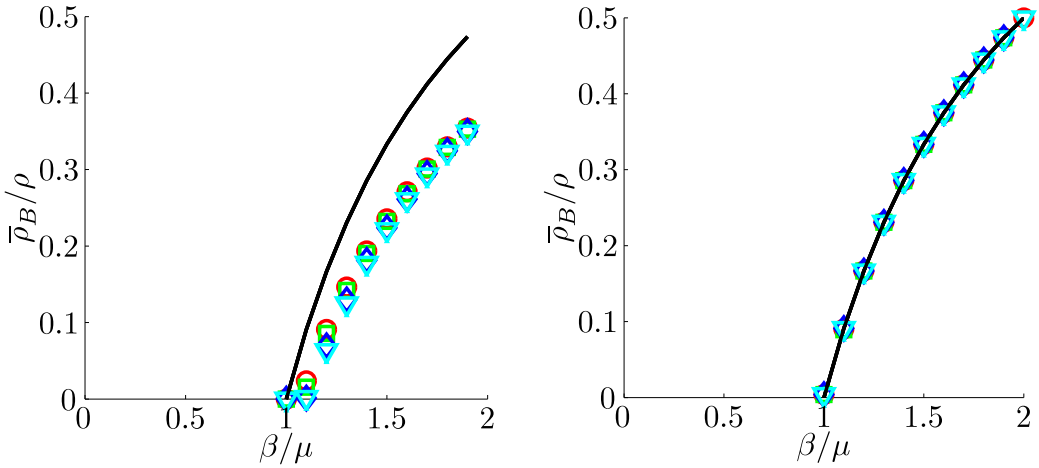

(a) Colizza (stochastic, μ and β unkown). Simulation results read directly from figure in Ref. [8], analytical results superimposed by us.

(b) Lund [2] (deterministic, $\mu = 0.1$)

Figure 4.3: Comparison of (a) Colizza's and (b) Lund's simulation results for type II reactions, with $\rho = 20$ and $D_B = 1$. Lines indicate analytical result (Eq. (4.21)), symbols are simulation results. Each symbol with properties (γ, V, D_A): Circles $\circ$ (2.5, 10^4, 1), squares $\square$ (3.0, 10^4, 1), diamonds $\diamond$ (2.5, 10^4, 0) and triangles $\triangledown$ (3.0, 10^4, 0).

than with high ones, shown in Fig. 4.4(b). By lowering the reaction coefficients, the position of the phase transition is also more accurately determined. This should serve as a confirmation that it is not the implementation in itself that causes the errors, but instead the exceedingly high values of the reaction coefficients μ and β.

For type II, similar stochastic results are shown in Fig. 4.5. High reaction coefficients ($\mu = 0.4$) also in this case lead to results similar to those of Ref. [8], which indicates that this is the reason why their results are not correct. The results for lower reaction coefficients, in Fig. 4.5(c), are once again far closer to the analytical solution, and has a more accurate phase transition.

The stochastic simulations performed to obtain the results in figures 4.4 and 4.5 are (with our implementation) quite computationally expensive, far more expensive than the discretization of the differential equations. With our implementation, the difference is on the order of 10^2. Higher reaction coefficients help reduce the time needed for simulations, because the stationary state is reached in fewer simulation steps. It is therefore tempting to perform simulations with high reaction rates, at the expense of the accuracy of the results. This may be the reason why Colizza *et al.* apparently have used such high rates.

Finally, we present simulation results for type M in Fig. 4.6. The simulation results accurately match the analytical mean-field predictions. We see that the stationary state $\overline{\rho}_B$ for the different cases all approach the stationary state of type II ($\overline{\rho}_B/\rho = 0.5$) as $\rho/\rho_\times$ increases. Since type M is similar to type II when $\rho \gg \rho_\times$, this is to be expected. On the other hand, the stationary state is sensitive to network topology when $\rho/\rho_\times$ is small. This

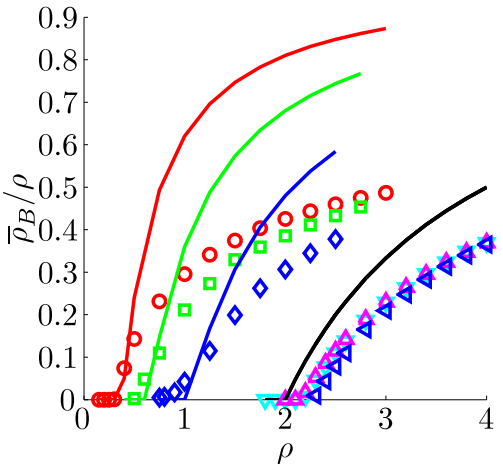

(a) Colizza (stochastic, μ and β unkown). Simulation results read directly from figure in Ref. [8], analytical results superimposed by us.

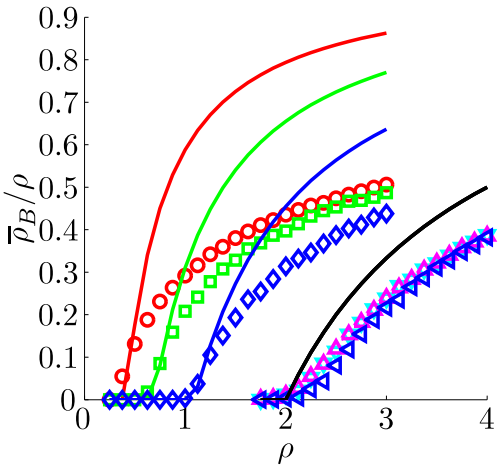

(b) Lund (stochastic, $\mu = 0.4$, $\beta = 0.2$)

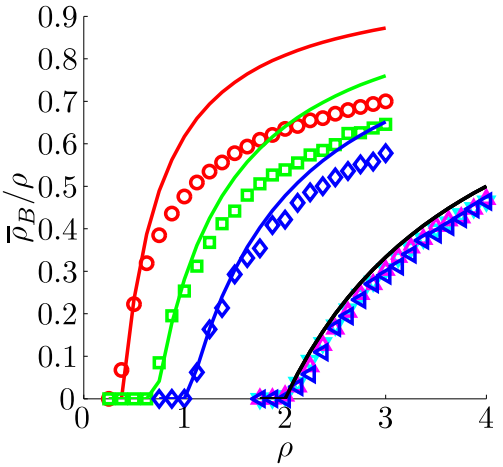

(c) Lund (stochastic, $\mu = 0.1$, $\beta = 0.05$)

Figure 4.4: Comparison of (a) Colizza's [8] and (b)-(c) Lund's stochastic simulation results for type I reactions, with $\mu/\beta = 2$ and $D_B = 1$. Lines indicate analytical results (Eqs. (4.14) and (4.20)), symbols are simulation results. Each symbol with properties (γ, V, D_A): Circles $\circ$ (2.5, 10^5, 1), squares $\square$ (2.5, 10^4, 1), diamonds $\diamond$ (2.5, 10^3, 1), downward triangle $\triangledown$ (2.5, 10^4, 0), upward triangle $\triangle$ (2.5, 10^5, 0), leftward triangle $\triangleleft$ (3.0, 10^4, 0).

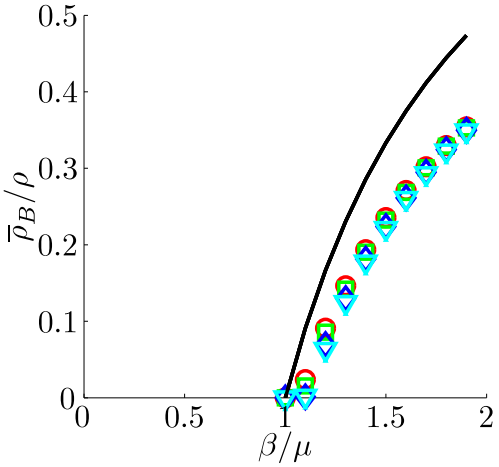

(a) Colizza (stochastic, μ and β unkown). Simulation results read directly from figure in Ref. [8], analytical results superimposed by us.

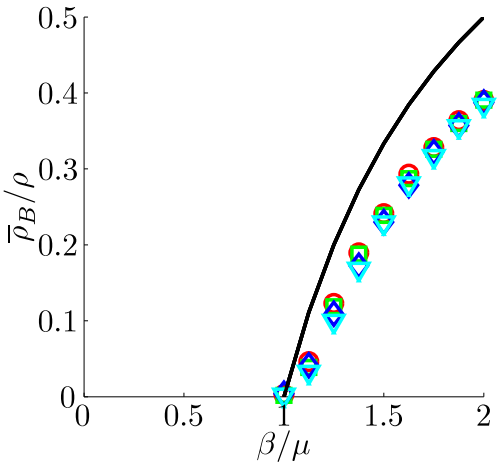

(b) Lund (stochastic, $\mu = 0.4$)

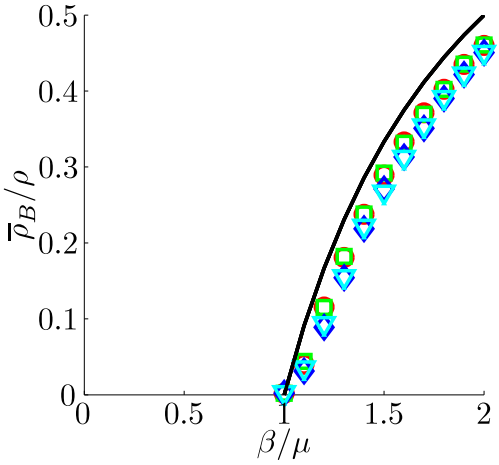

(c) Lund (stochastic, $\mu = 0.05$)

Figure 4.5: Comparison of (a) Colizza's [8] and (b)-(c) Lund's stochastic simulation results for type II reactions, with $\rho = 20$ and $D_B = 1$. Lines indicate analytical result (Eq. (4.21)), symbols are simulation results. Each symbol with properties (γ, V, D_A): Circles $\circ$ (2.5, 10^4, 1), squares $\square$ (3.0, 10^4, 1), diamonds $\diamond$ (2.5, 10^4, 0) and triangles $\triangledown$ (3.0, 10^4, 0).

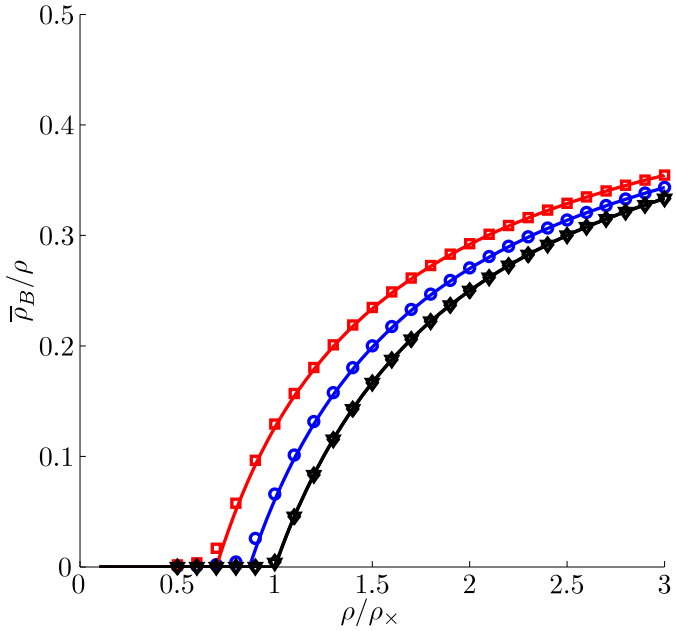

(a) Scale-free network, $\gamma = 2.5$

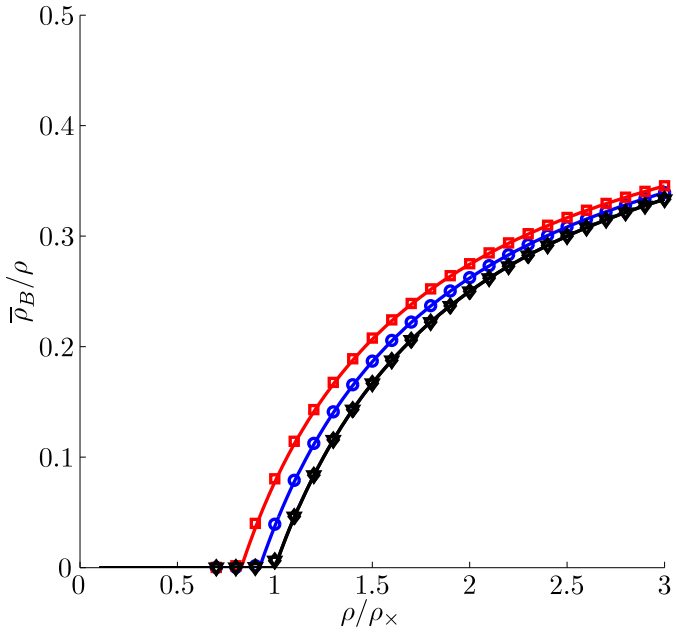

(b) Scale-free network, $\gamma = 3.0$

Figure 4.6: Simulation results for type M reactions, with $D_B = 1$ and $\beta/\mu = 2$. Lines indicate analytical result (Eqs. (4.18) and (4.22)), symbols are simulation results. Each symbol with properties (V, D_A): Circles ○ (10^4, 1), squares □ (10^2, 1), diamonds ◇ (10^4, 0) and triangles ▽ (10^2, 0).

is expected since type M is similar to type I when $\rho/\rho_\times$ is small.

Fig. 4.6 shows results for two scale-free networks with exponents $\gamma = 2.5$ (Fig. 4.6(a)) and $\gamma = 3.0$ (Fig. 4.6(b)). We see that the results are more sensitive to network size when $\gamma = 2.5$ than with $\gamma = 3.0$. This is because a higher γ gives more homogeneous degrees, which in turn will increase the critical density ρ_c. This can be seen from equation (4.22).

4.2 Continuous-time reaction-diffusion

As pointed out by Saldaña [10], the approach of Colizza *et al.* has no well-defined continuous-time limit. The equations they present do not include any time interval τ so that the equations can be considered in the limit $\tau \to 0$. We will now do an approach similar to that of Colizza *et al.*, but introducing a time interval for each step.

We let the time step for each reaction and diffusion be τ. That is, reactions occur in a time interval $[t, t+\tau)$, followed by diffusion in the time interval $[t+\tau, t+2\tau)$. The discrete time equations for reactions are then

$$\rho_{A,k}(t+\tau) = \rho_{A,k}(t) + \tau\mu\rho_{B,k}(t) - \tau\beta\Gamma_k(t) \,, \tag{4.23a}$$
$$\rho_{B,k}(t+\tau) = (1-\tau\mu)\rho_{B,k}(t) + \tau\beta\Gamma_k(t) \,. \tag{4.23b}$$

and the discrete time equations for diffusion are

$$\rho_{A,k}(t+2\tau) = (1-\tau D_A)\rho_{A,k}(t+\tau) + \tau D_A \frac{k}{\langle k\rangle}\sum_{k'} p(k')\rho_{A,k'}(t+\tau) \,, \tag{4.24a}$$
$$\rho_{B,k}(t+2\tau) = (1-\tau D_B)\rho_{B,k}(t+\tau) + \tau D_B \frac{k}{\langle k\rangle}\sum_{k'} p(k')\rho_{B,k'}(t+\tau) \,. \tag{4.24b}$$

By substituting the expression for $\rho_{A,k}(t+\tau)$ and $\rho_{B,k}(t+\tau)$ from Eqs. (4.23) into Eqs. (4.24) we get

$$\begin{aligned}\rho_{A,k}(t+2\tau) &= (1-\tau D_A)(\rho_{A,k}(t) + \tau\mu\rho_{B,k}(t) - \tau\beta\Gamma_k(t)) \\ &\quad + \tau D_A \frac{k}{\langle k\rangle}\sum_{k'} p(k')(\rho_{A,k}(t) + \tau\mu\rho_{B,k}(t) - \tau\beta\Gamma_k(t)) \,, \end{aligned}\tag{4.25a}$$
$$\begin{aligned}\rho_{B,k}(t+2\tau) &= (1-\tau D_B)((1-\tau\mu)\rho_{B,k}(t) + \tau\beta\Gamma_k(t)) \\ &\quad + \tau D_B \frac{k}{\langle k\rangle}\sum_{k'} p(k')((1-\tau\mu)\rho_{B,k}(t) + \tau\beta\Gamma_k(t)) \,. \end{aligned}\tag{4.25b}$$

After doing the sums over k', we get

$$\begin{aligned}\rho_{A,k}(t+2\tau) &= (1-\tau D_A)(\rho_{A,k}(t) + \tau\mu\rho_{B,k}(t) - \tau\beta\Gamma_k(t)) \\ &\quad + \tau D_A \frac{k}{\langle k\rangle}(\rho_A(t) + \tau\mu\rho_B(t) - \tau\beta\Gamma(t)) \,, \end{aligned}\tag{4.26a}$$
$$\begin{aligned}\rho_{B,k}(t+2\tau) &= (1-\tau D_B)((1-\tau\mu)\rho_{B,k}(t) + \tau\beta\Gamma_k(t)) \\ &\quad + \tau D_B \frac{k}{\langle k\rangle}((1-\tau\mu)\rho_B(t) + \tau\beta\Gamma(t)) \,. \end{aligned}\tag{4.26b}$$

Now we approximate the continuous time derivatives $\partial_t \rho_{A,k}(t)$ and $\partial_t \rho_{B,k}(t)$ with the standard forward difference (over two time steps),

$$\partial_t \rho_{A,k}(t) \approx \frac{\rho_{A,k}(t+2\tau) - \rho_{A,k}(t)}{2\tau} , \tag{4.27a}$$

$$\partial_t \rho_{B,k}(t) \approx \frac{\rho_{B,k}(t+2\tau) - \rho_{B,k}(t)}{2\tau} . \tag{4.27b}$$

Hence from Eqs. (4.26) we get

$$\begin{aligned} \partial_t \rho_{A,k}(t) = {} & \frac{1-\tau D_A}{2}(\mu\rho_{B,k}(t) - \beta\Gamma_k(t)) - \frac{D_A}{2}\rho_{A,k}(t) \\ & + \frac{D_A}{2}\frac{k}{\langle k\rangle}\left[\rho_A(t) + \tau\mu\rho_B(t) - \tau\beta\Gamma(t)\right] , \end{aligned} \tag{4.28a}$$

$$\begin{aligned} \partial_t \rho_{B,k}(t) = {} & \frac{1-\tau D_B}{2}(-\mu\rho_{B,k}(t) + \beta\Gamma_k(t)) - \frac{D_B}{2}\rho_{B,k}(t) \\ & + \frac{D_B}{2}\frac{k}{\langle k\rangle}\left[(1-\tau\mu)\rho_B(t) + \tau\beta\Gamma(t)\right] . \end{aligned} \tag{4.28b}$$

When letting $\tau = 1$ one can easily see that Eqs. (4.28) is *almost* equivalent to Colizza's equations (4.8) apart from a factor 2. This factor appears because Colizza *et al.* have defined the time derivative differently, as pointed out earlier.

To achieve a continuous time derivative, one would typically let the time step τ decrease, *i.e.* $\tau \to 0$. The limit $\tau \to 0$ insures that events are mutually exclusive (as pointed out by Saldaña [10]), *i.e.* a single particle is subject to at most one event in each time step. Taking this limit leads to the following differential equations for $\rho_{A,k}(t)$ and $\rho_{B,k}(t)$:

$$\partial_t \rho_{A,k}(t) = \frac{1}{2}\left[\mu\rho_{B,k}(t) - \beta\Gamma_k(t) - D_A\rho_{A,k}(t) + D_A\frac{k}{\langle k\rangle}\rho_A(t)\right] , \tag{4.29a}$$

$$\partial_t \rho_{B,k}(t) = \frac{1}{2}\left[-\mu\rho_{B,k}(t) + \beta\Gamma_k(t) - D_B\rho_{B,k}(t) + D_B\frac{k}{\langle k\rangle}\rho_B(t)\right] . \tag{4.29b}$$

This is similar to the master equation for a continuous reaction-diffusion process, $\partial_t \boldsymbol{\rho} = \mathbf{D}\nabla^2\boldsymbol{\rho} + \boldsymbol{R}(\boldsymbol{\rho})$. The difference is a factor $\frac{1}{2}$, because reactions only occur half of the time, and similar for diffusion.

We proceed with Eqs. (4.29), only replacing all rates $r \in \{\mu, \beta, D_A, D_B\}$ in Eqs. (4.29) with $2r$. This would have been the result if we had let diffusion and reaction occur simultaneously.

$$\partial_t \rho_{A,k}(t) = \mu\rho_{B,k}(t) - \beta\Gamma_k(t) - D_A\rho_{A,k}(t) + D_A\frac{k}{\langle k\rangle}\rho_A(t) , \tag{4.30a}$$

$$\partial_t \rho_{B,k}(t) = -\mu\rho_{B,k}(t) + \beta\Gamma_k(t) - D_B\rho_{B,k}(t) + D_B\frac{k}{\langle k\rangle}\rho_B(t) . \tag{4.30b}$$

We now want to solve for the stationary state $\overline{\rho}_{B,k}$, *i.e.* when $\partial_t \rho_{A,k}(t) = \partial_t \rho_{B,k}(t) = 0$. This leads to the equations

$$-D_A \overline{\rho}_{A,k} + D_A \frac{k}{\langle k \rangle} \overline{\rho}_A + \mu \overline{\rho}_{B,k} - \beta \overline{\Gamma}_k = 0 \,, \tag{4.31a}$$

$$-D_B \overline{\rho}_{B,k} + D_B \frac{k}{\langle k \rangle} \overline{\rho}_B - \mu \overline{\rho}_{B,k} + \beta \overline{\Gamma}_k = 0 \,. \tag{4.31b}$$

We can now compare these equations with the ones resulting from Colizza's approach. Dividing Eqs. (4.11) by $(1 - D_A)$ and $(1 - D_B)$, respectively, yields

$$-\frac{D_A}{1 - D_A} \overline{\rho}_{A,k} + \frac{D_A}{1 - D_A} \frac{k}{\langle k \rangle} \overline{\rho}_A + \mu \overline{\rho}_{B,k} - \beta \overline{\Gamma}_k = 0 \,, \tag{4.32a}$$

$$-\frac{D_B}{1 - D_B} \overline{\rho}_{B,k} + \frac{D_B}{1 - D_B} \frac{k}{\langle k \rangle} \overline{\rho}_B - \mu \overline{\rho}_{B,k} + \beta \overline{\Gamma}_k = 0 \,. \tag{4.32b}$$

We can see that the equations are very similar, except the diffusion factor. The relation between the two diffusion constants $D_{A,\text{disc}}$ (discrete time) and $D_{B,\text{cont}}$ (continuous time) is

$$D_{A,\text{cont}} = \frac{D_{A,\text{disc}}}{1 - D_{A,\text{disc}}} \,, \tag{4.33}$$

and similarly for D_B. An interesting point to note is that a discrete diffusion constant $D_{A,\text{disc}} = 1$ implies a continuous diffusion constant $D_{A,\text{cont}} \to \infty$.

Another way to explain the difference between the discrete and continuous equations, is to investigate how the equations are affected by changing the diffusion and reaction rates. One would intuitively expect that by scaling all rates (D_A, D_B, μ, β) with the same factor, one would just re-scale time, leaving the stationary state unchanged. From the continuous equation, (4.31), we see that the stationary state is unchanged by scaling the rates. For discrete time, however, Eq. (4.32) reveals that a scaling of the rates would affect diffusion and reaction differently.

We have now explained some of the similarities and differences between the analytical approaches with continuous and discrete time. Apart from a different diffusion factor, the equations are identical. Since the continuous time equations are perhaps more intuitive and a better mathematical description of a continuous reaction-diffusion process, we prefer this approach to the discrete time approach, and use it in further calculations. We will now make an attempt to solve for the stationary states $\overline{\rho}_{B,k}$ and $\overline{\rho}_B$, this time for any values of D_A and D_B.

4.3 Solving for the stationary state $\overline{\rho}_B$

We choose to continue with the continuous-time equations (4.31), as the results can easily be translated to the discrete-time situation using Eq. (4.33). From now on we let D_A and D_B implicitly denote the continuous diffusion coefficients ($D_{A,\text{cont}}$ and $D_{B,\text{cont}}$). We will make an attempt to solve for all values of D_A and D_B, and also for the newly introduced type M. Solving explicitly for $\overline{\rho}_{A,k}$ and $\overline{\rho}_{B,k}$ is not as easy as in Colizza's expressions. We therefore try to express $\overline{\rho}_{A,k}$ and $\overline{\rho}_{B,k}$ as series expansions in powers of k:

$$\overline{\rho}_{A,k} = \sum_{i=0}^{\infty} a_i k^i \,, \tag{4.34a}$$

$$\overline{\rho}_{B,k} = \sum_{i=0}^{\infty} b_i k^i \,. \tag{4.34b}$$

Adding equations (4.31a) and (4.31b) gives us a relation between $\overline{\rho}_{A,k}$ and $\overline{\rho}_{B,k}$:

$$D_A(\overline{\rho}_{A,k} - \frac{k}{\langle k\rangle}(\rho - \overline{\rho}_B)) = -D_B(\overline{\rho}_{B,k} - \frac{k}{\langle k\rangle}\overline{\rho}_B)\,. \tag{4.35}$$

Inserting the series expansions into Eq. (4.35) gives a relation between a_i and b_i:

$$a_i = \begin{cases} -\frac{D_B}{D_A} b_i \,, & \text{if } i \neq 1, \\ \frac{\rho}{\langle k\rangle} - \frac{D_B}{D_A} b_1 - \frac{\overline{\rho}_B}{\langle k\rangle}(1 - \frac{D_B}{D_A}) \,, & \text{if } i = 1. \end{cases} \tag{4.36}$$

To continue we have to insert an expression for the reaction kernel $\overline{\Gamma}_k$, depending on the reaction type.

4.3.1 Type I

For type I, the reaction kernel (in the stationary state) reads $\overline{\Gamma}_k = \overline{\rho}_{A,k}\overline{\rho}_{B,k}$. Inserting this and the series expansion (4.34) into Eq. (4.31b), we get

$$-(D_B + \mu)\sum_{i=0}^{\infty} b_i k^i + D_B \frac{k}{\langle k\rangle}\overline{\rho}_B + \beta \sum_{i=0}^{\infty}\left[a_i k^i \sum_{j=0}^{\infty} b_j k^j \right] = 0. \tag{4.37}$$

We then continue by solving Eqs. (4.37) for every power of k separately.

- **0th order**

  With only terms of order $k^0 = 1$, equation (4.37) gives us an expression for b_0:

$$-(D_B + \mu)b_0 + \beta a_0 b_0 = -(D_B + \mu)b_0 - \beta\frac{D_B}{D_A} b_0^2 = 0 \,,$$

$$b_0 = 0 \;\vee\; b_0 = -\frac{D_A(D_B + \mu)}{D_B \beta} \,.$$

  We must have that $\overline{\rho}_{B,k} = 0 \;\forall\; k$ when $\overline{\rho}_B = 0$, which implies that $b_0 = a_0 = 0$.

- **1st order**

  With terms of order k^1, equation (4.37) yields

$$-(D_B+\mu)b_1 + D_B\frac{\overline{\rho}_B}{\langle k\rangle} = 0\ ,$$
$$b_1 = \frac{D_B\overline{\rho}_B}{\langle k\rangle(D_B+\mu)}\ . \tag{4.38}$$

  From Eq. (4.36) we get an expression for a_1:

$$a_1 = \frac{\rho}{\langle k\rangle} - \frac{\overline{\rho}_B}{\langle k\rangle}\left(1 - \frac{D_B\mu}{D_A(D_B+\mu)}\right)\ . \tag{4.39}$$

  Since we want to be able to solve for $\overline{\rho}_B$, we expand each coefficient a_i and b_i in powers of $\overline{\rho}_B$:

$$a_i = \sum_{j=0}^{\infty} a_{i,j}\overline{\rho}_B^j\ , \tag{4.40a}$$
$$b_i = \sum_{j=0}^{\infty} b_{i,j}\overline{\rho}_B^j\ . \tag{4.40b}$$

  Using this notation, Eq. (4.39) implies

$$a_{1,j} = \begin{cases} \frac{\rho}{\langle k\rangle}\ , & \text{if } j=0,\\ \frac{1}{\langle k\rangle}\left(\frac{D_B\mu}{D_A(D_B+\mu)} - 1\right)\ , & \text{if } j=1,\\ 0\ , & \text{otherwise.}\end{cases} \tag{4.41}$$

  and Eq. (4.38) gives

$$b_{1,j} = \begin{cases} \frac{D_B}{\langle k\rangle(D_B+\mu)}\ , & \text{if } j=1,\\ 0\ , & \text{otherwise.}\end{cases} \tag{4.42}$$

- **Higher orders**

  For higher orders ($i > 1$), we can derive equations which relate a_i and b_i to lower order coefficients. Equation (4.37) gives us

$$-(D_B+\mu)b_i + \beta\sum_{l=1}^{i-1} a_l b_{i-l} = 0\ ,$$
$$b_i = \frac{\beta}{D_B+\mu}\sum_{l=1}^{i-1} a_l b_{i-l} = \frac{\beta}{D_B+\mu}\sum_{l=1}^{i-1}\sum_{m=0}^{\infty}\sum_{n=0}^{\infty} a_{l,m}b_{i-l,n}\overline{\rho}_B^{m+n}\ .$$

Looking only at the j-th power of $\overline{\rho}_B$, we must have $m + n = j$, or $n = j - m$. This gives an expression for $b_{i,j}$:

$$b_{i,j} = \frac{\beta}{D_B + \mu} \sum_{l=1}^{i-1} \sum_{m=0}^{j} a_{l,m} b_{i-l,j-m} \,. \tag{4.43}$$

Eq. (4.36) relates $a_{i,j}$ to $b_{i,j}$:

$$a_{i,j} = -\frac{D_B \beta}{D_A(D_B + \mu)} \sum_{l=1}^{i-1} \sum_{m=0}^{j} a_{l,m} b_{i-l,j-m} \,.$$

From these equations we can see that b_i is only dependent on lower degree coefficients, *i.e.* a_l and b_l where $l < i$.

We can now calculate the density of B particles in the stationary state using $\overline{\rho}_B = \sum_k p(k)\overline{\rho}_{B,k}$:

$$\begin{aligned}\overline{\rho}_B &= \sum_k p(k)\overline{\rho}_{B,k} = \sum_k p(k) \sum_{i=0}^{\infty} b_i k^i = \sum_k p(k) \left[\sum_{i=0}^{\infty} k^i \left(\sum_{j=0}^{\infty} b_{i,j} \overline{\rho}_B^j \right) \right] \\ &= \sum_{i=0}^{\infty} \langle k^i \rangle \left(\sum_{j=0}^{\infty} b_{i,j} \overline{\rho}_B^j \right)\end{aligned}$$

We already know that $b_{i,0} = 0$, so we start the summation at $j = 1$. We divide by $\overline{\rho}_B$ and get

$$1 = \sum_{j=1}^{\infty} \overline{\rho}_B^{(j-1)} \sum_{i=0}^{\infty} \langle k^i \rangle b_{i,j} = \sum_{j=0}^{\infty} \overline{\rho}_B^j \sum_{i=0}^{\infty} \langle k^i \rangle b_{i,j+1} \,.$$

Rearranging this finally yields

$$\left(\sum_{j=0}^{\infty} \overline{\rho}_B^j \sum_{i=0}^{\infty} \langle k^i \rangle b_{i,j+1} \right) - 1 = 0 \,. \tag{4.44}$$

By terminating the j-sum at some finite n, one retrieves an nth order equation which can be solved analytically or numerically.

Simulation results

Simulation results, compared to solutions of Eq. (4.44), for different cases are shown in Figure 4.7. A plot of $\overline{\rho}_{B,k}$ as function of k for the same cases is shown in Fig. 4.8. As we see, the analytical solution is good for several different values of D_A and D_B. Colizza's expressions for $D_{A,\text{disc}} = D_{B,\text{disc}} = 1$, *i.e.* $D_{A,\text{cont}} = D_{B,\text{cont}} = \infty$, are shown to illustrate the difference between these and our series expansions. In these figures we have used $\gamma = 2.5$, but simulations have also been performed for other γs, giving similar results.

We see that the difference from Colizza's expressions is largest for the largest network ($V = 10^4$). This is because a larger network typically has higher degree fluctuations, and thus higher moments $\langle k^i \rangle$. We also note that the phase transition seems to move left (lower critical density ρ_c), while the stationary state for higher densities is lower than for $D_A = D_B = \infty$.

However, the analytical solution encounters problems when D_A and D_B are small (on the same order as μ and β), as shown in Fig. 4.7(d). For the same case, Fig. 4.8(d) shows how the analytical expression diverges for high node degrees k. However, when D_A and D_B are small, the mean-field approximation is not a good approximation either. As Fig. 4.8(d) shows, the spread in number of B particles for nodes with equal degree is substantial, especially for low degree nodes. With faster diffusion ($D_A = 0.7$, $D_B = 1$), the spread in for each degree is much less, *i.e.* the mean-field approximation is better with fast than with slow diffusion. This is discussed in the next section.

Since the mean-field approximation is not exact, one cannot expect the series expansion to be exact either. In addition, a high order expansion will be sensitive to high degrees. This is seen in Fig. 4.8(d), where the analytical solution is diverging for high degrees. The simulations show a clear deviation from the linear function $\overline{\rho}_{B,k} = \overline{\rho}_B k/\langle k \rangle$. With only a finite number of terms from the series expansion, this approach is best when the density $\overline{\rho}_{B,k}$ is almost linear in k, *i.e.* when the diffusion dominates over reaction and the mean-field approximation is good.

Validity of the mean-field approximation

As Fig. 4.8 shows, nodes with the same degree have a similar, but not exactly the same, number of B particles, which indicates that the mean-field approximation is not perfect. We will therefore try to show why this is the case. By going back to the equations for a single node, we can readily discover if the mean-field approximation is correct or not. The differential equation for $N_B(i,t)$, *i.e.* the number of B particles at node i at time t, is

$$\frac{dN_B(i,t)}{dt} = -(D_B + \mu)N_B(i,t) + \beta N_A(i,t)N_B(i,t) + D_B \sum_{j \in U(i)} \frac{N_B(j,t)}{k_j}, \tag{4.45}$$

where $U(i)$ denotes the set of neighbors to node i. In the mean-field approximation, $\overline{N}_B(i) = \overline{\rho}_{B,k_i}$, which yields

$$-(D_B + \mu)\overline{\rho}_{B,k_i} + \beta \overline{\rho}_{A,k_i}\overline{\rho}_{B,k_i} + D_B \sum_{j \in U(i)} \frac{\overline{\rho}_{B,k_j}}{k_j} = 0\,. \tag{4.46}$$

We know that the previously presented stationary state, $\overline{\rho}_{B,k}$, satisfies the equation

$$-(D_B + \mu)\overline{\rho}_{B,k} + \beta \overline{\rho}_{A,k}\overline{\rho}_{B,k} + D_B \frac{k}{\langle k \rangle}\overline{\rho}_B = 0\,. \tag{4.47}$$

Hence, by comparing the two equations (4.46) and (4.47), we see that Eq. (4.46) can only be satisfied if

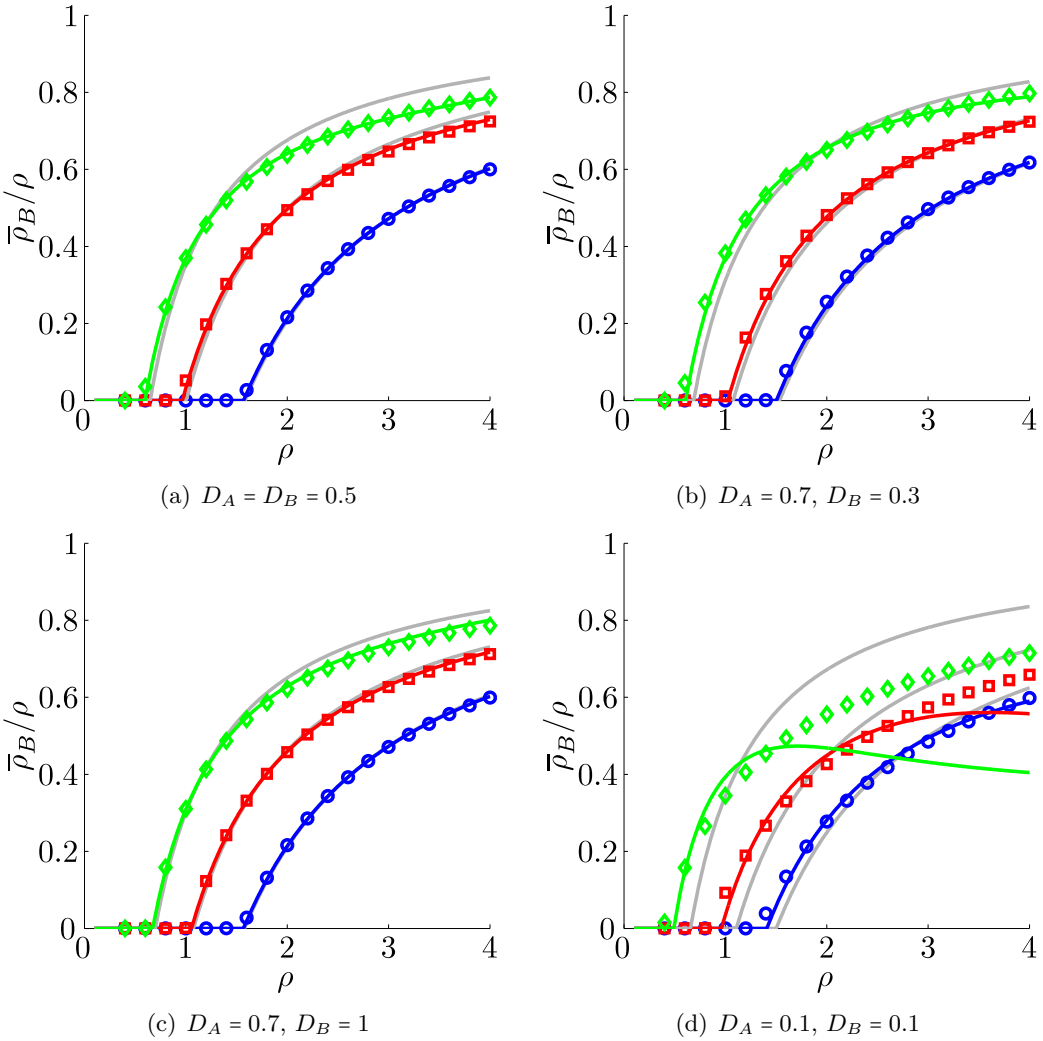

(a) $D_A = D_B = 0.5$

(b) $D_A = 0.7$, $D_B = 0.3$

(c) $D_A = 0.7$, $D_B = 1$

(d) $D_A = 0.1$, $D_B = 0.1$

Figure 4.7: Stationary state for type I reactions, with $\mu = 0.02$ and $\beta = 0.01$. Grey lines are Colizza's analytical results ($D_A = D_B = \infty$, Eq. (4.20b)), colored lines indicate analytical result (4th order of Eq. (4.44)), symbols are simulation results. Each symbol with network size (V): Circles $\circ$ (10^2), squares $\square$ (10^3) and diamonds $\diamond$ (10^4). All networks are scale-free with $\gamma = 2.5$.

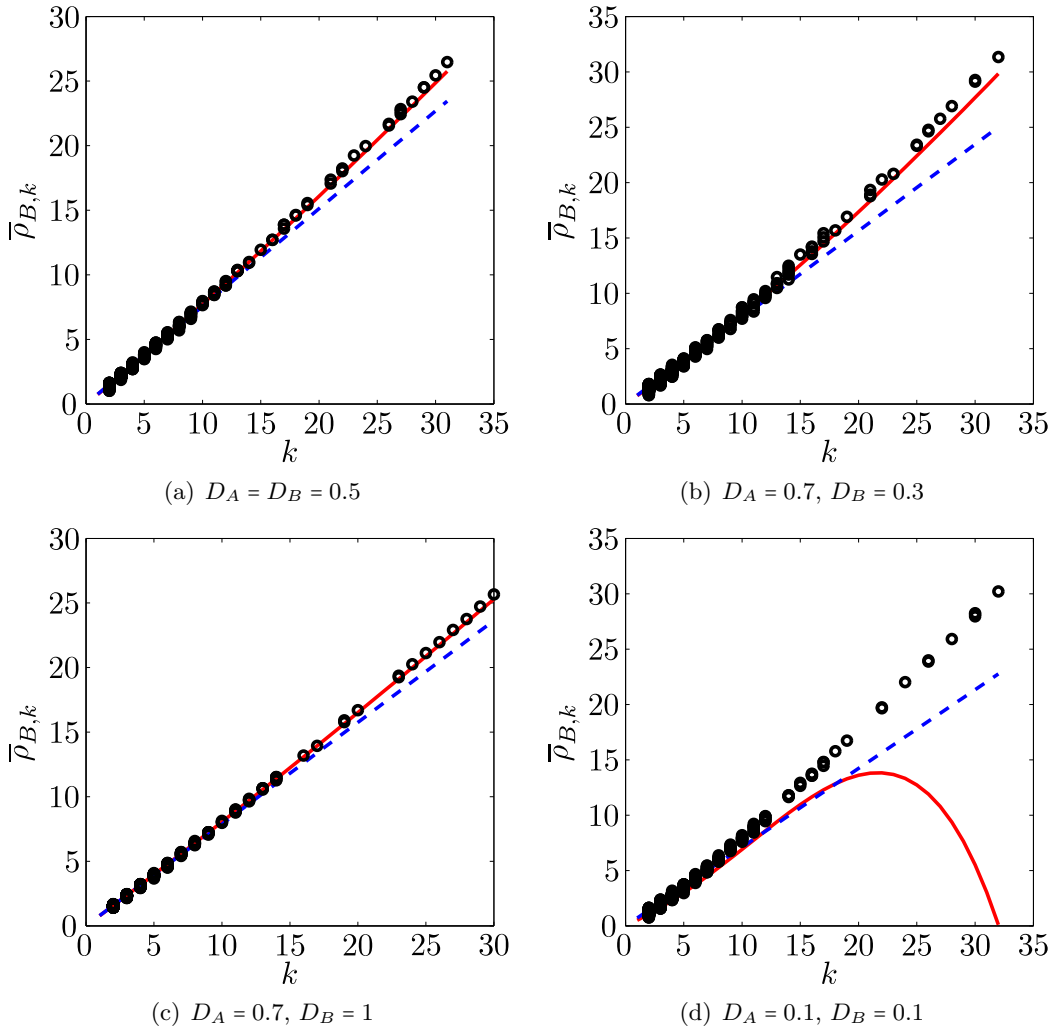

(a) $D_A = D_B = 0.5$

(b) $D_A = 0.7$, $D_B = 0.3$

(c) $D_A = 0.7$, $D_B = 1$

(d) $D_A = 0.1$, $D_B = 0.1$

Figure 4.8: Density of B particles, $\overline{\rho}_{B,k}$, as function of degree k, with $\mu = 0.02$, $\beta = 0.01$ and $\rho = 4$. The network is scale-free with $V = 1000$ and $\gamma = 2.5$. Dashed lines are linear ($\overline{\rho}_{B,k} = k/\langle k \rangle \overline{\rho}_B$), solid lines are analytical results (4th order of Eq. (4.34b)). Each symbol corresponds to a node with it's degree and number of B particles in stationary state.

$$\frac{k_i}{\langle k \rangle}\overline{\rho}_B = \sum_{j \in U(i)} \frac{\overline{\rho}_{B,k_j}}{k_j} \, .$$

Inserting the series expansion of $\overline{\rho}_{B,k}$ yields

$$\frac{k_i}{\langle k \rangle}\sum_{l=1}^{\infty} b_l \langle k^l \rangle = \sum_{j \in U(i)} \sum_{l=1}^{\infty} b_l k_j^{l-1} \, . \tag{4.48}$$

Since k_j, that is the degree of a neighbor node j, may vary, this equation is not always (and possibly never) exactly satisfied. Thus, one may conclude that *the mean-field approximation is not exactly correct for type I reactions.*

Although the mean-field approximation is not exactly correct, it is instructive to investigate when it represents a reasonable approximation. Eq. (4.48) is satisfied if $b_i = 0$ for $i > 1$, *i.e.* $\overline{\rho}_{B,k} \sim k$. This is the case if we have only diffusion, when $D_B, D_A \gg \mu, \rho\beta$.

4.3.2 Type II

For type II, the reaction kernel (in the stationary state) reads $\overline{\Gamma}_k = \overline{\rho}_{A,k}\overline{\rho}_{B,k}/\overline{\rho}_k$. Inserting this into Eq. (4.31b), we get

$$-(D_B + \mu)\overline{\rho}_{B,k} + D_B \frac{k}{\langle k \rangle}\overline{\rho}_B + \beta \frac{\overline{\rho}_{A,k}\overline{\rho}_{B,k}}{\overline{\rho}_{A,k} + \overline{\rho}_{B,k}} = 0. \tag{4.49}$$

One could continue by making the same approach using series expansions as in section 4.3.1, but instead we then make a clever guess by assuming that $\overline{\rho}_{A,k}$ and $\overline{\rho}_{B,k}$ are of the same form as with discrete time;

$$\overline{\rho}_{A,k} = \frac{k}{\langle k \rangle}\overline{\rho}_A,$$
$$\overline{\rho}_{B,k} = \frac{k}{\langle k \rangle}\overline{\rho}_B.$$

Inserting this into (4.49) yields

$$-(D_B + \mu)\overline{\rho}_B + D_B\overline{\rho}_B + \beta \frac{\overline{\rho}_A\overline{\rho}_B}{\overline{\rho}_A + \overline{\rho}_B} =$$
$$\overline{\rho}_B\left(-\mu + \beta\frac{\rho - \overline{\rho}_B}{\rho}\right) = 0,$$
$$\overline{\rho}_B = \rho\left(1 - \frac{\mu}{\beta}\right),$$

which is the same solution as Colizza *et al.* presented. In figure 4.9 we present simulation results together with this analytical result. The figure shows that the simulations match the analytical result exactly, regardless of the values of the diffusion constants D_A and D_B.

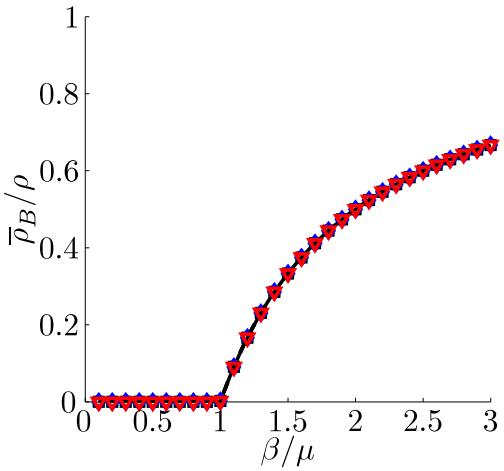

Figure 4.9: Stationary state for type II reactions, with $\mu = 0.1$ and $D_B = 0.5$. Solid line is analytical result, symbols are simulation results. Each symbol with network size and A diffusion constant (V, D_A): Circles ○ (10^3, 0.5), squares □ (10^4, 0.5), diamonds ◇ (10^3, 0) and triangles ▽ (10^4, 0). All networks are scale-free with $\gamma = 2.5$.

4.3.3 Type M

For type M, the reaction kernel is $\overline{\Gamma}_k = \frac{\overline{\rho}_{A,k}\overline{\rho}_{B,k}}{\rho_\times + \overline{\rho}_k}$ in the stationary state. Inserting this and the series expansions (4.34) into Eq. (4.31b), we get

$$-(D_B+\mu)\sum_{i=0}^{\infty} b_i k^i (\rho_\times + \sum_{j=0}^{\infty}(a_j+b_j)k^j) + D_B \frac{k}{\langle k\rangle}\overline{\rho}_B(\rho_\times + \sum_{i=0}^{\infty}(a_i+b_i)k^i) + \beta\sum_{i=0}^{\infty}\left[a_i k^i \sum_{j=0}^{\infty} b_j k^j\right] = 0. \tag{4.50}$$

We then continue by solving equation (4.50) for every power of k separately.

- **0th order**

  Similar arguments as for type I imply that $b_0 = a_0 = 0$.

- **1st order**

  With terms of order k^1, equation (4.50) yields

$$-(D_B+\mu)b_1\rho_\times + D_B\frac{\overline{\rho}_B\rho_\times}{\langle k\rangle} = 0\,,$$
$$b_1 = \frac{D_B\overline{\rho}_B}{\langle k\rangle(D_B+\mu)}\,, \tag{4.51}$$

and Eq. (4.36) gives us

$$a_1 = \frac{\rho}{\langle k \rangle} - \frac{\overline{\rho}_B}{\langle k \rangle}\left(1 - \frac{D_B \mu}{D_A(D_B + \mu)}\right) . \tag{4.52}$$

As with type I, we expand each coefficient a_i and b_i in powers of $\overline{\rho}_B$ (see Eqs. (4.40)). Using this notation, Eq. (4.52) implies

$$a_{1,j} = \begin{cases} \frac{\rho}{\langle k \rangle} , & \text{if } j = 0, \\ \frac{1}{\langle k \rangle}\left(\frac{D_B \mu}{D_A(D_B+\mu)} - 1\right) , & \text{if } j = 1, \\ 0 , & \text{otherwise.} \end{cases}$$

and Eq. (4.51)

$$b_{1,j} = \begin{cases} \frac{D_B}{\langle k \rangle (D_B+\mu)} , & \text{if } j = 1, \\ 0 , & \text{otherwise.} \end{cases}$$

- **Higher orders**

  For higher orders ($i > 1$), the coefficients a_i and b_i are once again dependent on lower order coefficients. Eq. (4.50) yields

$$-(D_B + \mu)(\rho_\times b_i + \sum_{l=1}^{i-1} b_{i-l}(a_l + b_l)) + D_B(a_{i-1} + b_{i-1})\frac{\overline{\rho}_B}{\langle k \rangle} + \beta \sum_{l=1}^{i-1} a_{i-l} b_l = 0 .$$

  Once again, we expand in powers of $\overline{\rho}_B$ and get

$$\begin{aligned} &- (D_B + \mu)\rho_\times \sum_{j=0}^{\infty} b_{i,j}\overline{\rho}_B^j + \sum_{l=1}^{i-1}\sum_{n=0}^{\infty}\sum_{m=0}^{\infty}(\beta a_{i-l,n} b_{l,m} - (D_B + \mu) b_{i-l,n}(a_{l,m} + b_{l,m}))\overline{\rho}_B^{m+n} \\ &+ \frac{D_B}{\langle k \rangle}\sum_{n=0}^{\infty}(a_{i-1,n} + b_{i-1,n})\overline{\rho}_B^{n+1} = 0 , \end{aligned}$$

  Collecting terms of the same power j yields

$$\begin{aligned} &- (D_B + \mu)\rho_\times b_{i,j} + \sum_{l=1}^{i-1}\sum_{m=0}^{j}(\beta a_{i-l,j-m} b_{l,m} - (D_B + \mu) b_{i-l,j-m}(a_{l,m} + b_{l,m})) \\ &+ \frac{D_B}{\langle k \rangle}(a_{i-1,j-1} + b_{i-1,j-1}) = 0 , \\ b_{i,j} = &\frac{1}{(D_B + \mu)\rho_\times}\Big(\sum_{l=1}^{i-1}\sum_{m=0}^{j}(\beta a_{i-l,j-m} b_{l,m} - (D_B + \mu) b_{i-l,j-m}(a_{l,m} + b_{l,m})) \\ &+ \frac{D_B}{\langle k \rangle}(a_{i-1,j-1} + b_{i-1,j-1})\Big) . \end{aligned}$$

From these equations we can see that b_i is only dependent on lower degree coefficients, *i.e.* a_l and b_l where $l < i$.

We can now use the same equation as for type I, Eq. (4.44), to calculate $\overline{\rho}_B$. However, it turns out that the sum $\sum_i b_i k^i$ is not converging, but alternating and diverging. The series is quite good in the limit where $\rho_\times \gg \rho$, *i.e.* almost type II, but in the limit $\rho_\times \to 0$, $b_{i,j}$ diverges. The reason for this can be seen from the last expression for $b_{i,j}$, from which it is evident that $\lim_{\rho_\times \to 0} |b_{i,j}| = \infty$.

Simulation results

Although the series expansion for type M does not seem to be instructive, we can still perform simulations and compare the results to the analytical results with $D_{B,\text{disc}} = 1$ and $D_{A,\text{disc}} \in \{0, 1\}$ (Eq. (4.18) and Eq. (4.22)). The results for several cases are shown in Fig. 4.10. As we see, the analytical expression matches the simulation results quite well. Eq. (4.18) and Eq. (4.22) are based on the assumption that $\rho_{B,k}$ is linear in k. We recall that this assumption is correct for type II reactions, regardless of the value of D_A and D_B, but not for type I reactions. As the results show, the analytical expression for type M is best when similar to type II ($\rho \gg \rho_\times$) and less good when similar to type I ($\rho \ll \rho_\times$). This is clearly seen in Fig. 4.10(b).

4.4 Phase transition

We can also examine how the location of the phase transition is affected by changing the parameters. This is interesting because it gives information about when there is a risk that the infection will spread and not die out.

4.4.1 Type I

Series expansion

One way of solving for the phase transition, is to use the series expansion approach presented earlier. We take Eq. (4.44) as our starting point,

$$\left(\sum_{j=0}^{\infty} \overline{\rho}_B^j \sum_{i=0}^{\infty} \langle k^i \rangle b_{i,j+1} \right) - 1 = 0 \,. \tag{4.53}$$

We want to find the phase transition, *i.e.* for which (critical) particle density $\rho = \rho_c$ we have no B particles in the stationary state. We insert $\overline{\rho}_B = 0$ into Eq. (4.53) and get

$$\left(\sum_{i=0}^{\infty} \langle k^i \rangle b_{i,1} \right) - 1 = 0 \,. \tag{4.54}$$

To solve for $\rho = \rho_c$, we need to know how $b_{i,1}$ relies on ρ. For $i = 1$, we know from Eq. (4.42) that

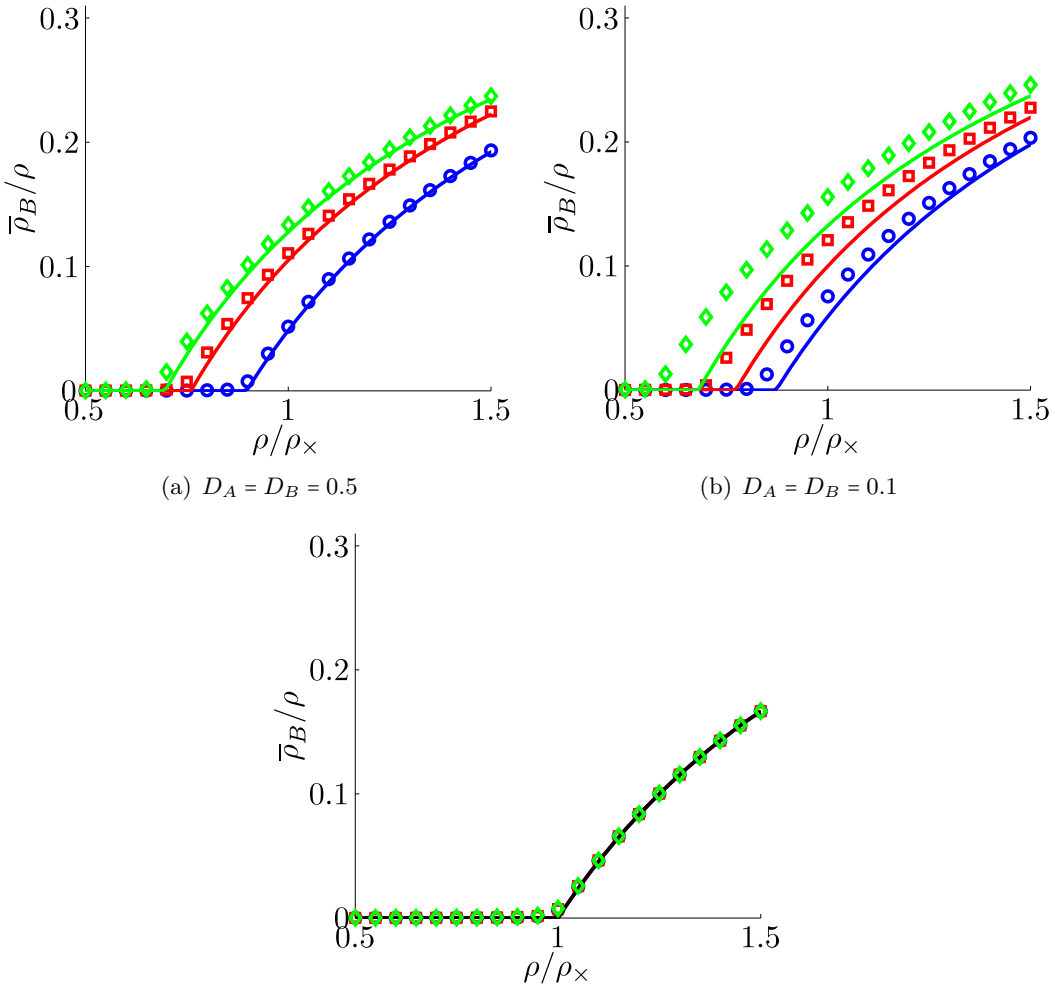

(a) $D_A = D_B = 0.5$

(b) $D_A = D_B = 0.1$

(c) $D_A = 0$, $D_B = 0.1$

Figure 4.10: Stationary state for type M reactions, with $\mu = 0.04$ and $\beta = 0.02$. Lines indicate analytical result for $D_B = \infty$ (Eq. (4.18) or Eq. (4.22)), symbols are simulation results. Each symbol with network size (V): Circles ○ (10^2), squares □ (10^3) and diamonds ◇ (10^4). All networks are scale-free with $\gamma = 2.5$.

$$b_{1,1} = \frac{D_B}{\langle k \rangle (D_B + \mu)} \, .$$

For orders higher than 1 ($i > 1$), Eq. (4.43) yields

$$b_{i,1} = \frac{\beta}{D_B + \mu} \sum_{l=1}^{i-1} (a_{l,0} b_{i-l,1} + a_{l,1} b_{i-l,0}) \, . \tag{4.55}$$

We continue by determining the factor $b_{i-l,0}$. With $j = 0$, Eq. (4.43) reads

$$b_{i,0} = \frac{\beta}{D_B + \mu} \sum_{l=1}^{i-1} a_{l,0} b_{i-l,0} \, .$$

From Eq. (4.42) we know that $b_{1,0} = 0$. Using this and the above equation for $b_{i,0}$ yields that $b_{i,0} = 0$ for all i. Eq. (4.36) then implies that $a_{i,0} = 0$ for all $i > 1$. This reduces Eq. (4.55) to

$$b_{i,1} = \frac{\beta}{D_B + \mu} a_{1,0} b_{i-1,1} \, . \tag{4.56}$$

Inserting $a_{1,0} = \rho_c / \langle k \rangle$ and $b_{1,1} = D_B / (\langle k \rangle (D_B + \mu))$ and using Eq. (4.56) recursively gives a general formula for $b_{i,1}$:

$$b_{i,1} = \left(\frac{\beta \rho_c}{(D_B + \mu) \langle k \rangle} \right)^{i-1} \frac{D_B}{\langle k \rangle (D_B + \mu)} \, .$$

Finally, inserting the expression for $b_{i,1}$ into Eq. (4.54), we get an equation for ρ_c:

$$\left(\sum_{i=1}^{\infty} \frac{\langle k^i \rangle}{\langle k \rangle^i} \frac{D_B}{D_B + \mu} \left(\frac{\beta}{D_B + \mu} \right)^{i-1} \rho_c^{i-1} \right) - 1 = 0 \, . \tag{4.57}$$

By terminating the i-sum at some finite integer n, one retrieves an nth order equation for ρ_c, which can be solved analytically or numerically. Higher degree n will presumably give a better result, although numerical difficulties may cause trouble for very high n.

Jacobian matrix

For comparison and to make sure the series expansion approach gives the correct result, we also present an approach based on a Jacobian matrix. This approach was briefly mentioned by Saldaña in Ref. [10], but not used for solving exactly for the critical density. More specifically, we look at the Jacobian matrix for the differential equations (4.30),

$$F_k = \partial_t \rho_{A,k}(t) = \mu \rho_{B,k}(t) - \beta \Gamma_k(t) - D_A \rho_{A,k}(t) + D_A \frac{k}{\langle k \rangle} \sum_{k'} p(k') \rho_{A,k'}(t) \, , \tag{4.58a}$$

$$G_k = \partial_t \rho_{B,k}(t) = -\mu \rho_{B,k}(t) + \beta \Gamma_k(t) - D_B \rho_{B,k}(t) + D_B \frac{k}{\langle k \rangle} \sum_{k'} p(k') \rho_{B,k'}(t) \, . \tag{4.58b}$$

We can determine the stability of the (trivial) stationary state $\overline{\rho}_A = \rho$, $\overline{\rho}_B = 0$ by examining the eigenvalues of the Jacobian matrix. If there are any eigenvalues $\lambda > 0$, this stationary state is unstable, and there exists a stationary state with $\overline{\rho}_B > 0$. In other words, when there exists an eigenvalue $\lambda > 0$, we are above the phase transition ($\rho > \rho_c$).

First, we simplify our notation by defining $A_k = \rho_{A,k}$, $B_k = \rho_{B,k}$ and the maximum degree $m = k_{\max}$. We then define our Jacobian matrix J as

$$J = \begin{pmatrix} \frac{\partial F_1}{\partial A_1} & \frac{\partial F_1}{\partial A_2} & \cdots & \frac{\partial F_1}{\partial A_m} & \frac{\partial F_1}{\partial B_1} & \cdots & \frac{\partial F_1}{\partial B_m} \\ \frac{\partial F_2}{\partial A_1} & \frac{\partial F_2}{\partial A_2} & \cdots & \frac{\partial F_2}{\partial A_m} & \frac{\partial F_2}{\partial B_1} & \cdots & \frac{\partial F_2}{\partial B_m} \\ \vdots & \vdots & \ddots & \vdots & \vdots & \ddots & \vdots \\ \frac{\partial F_m}{\partial A_1} & \frac{\partial F_m}{\partial A_2} & \cdots & \frac{\partial F_m}{\partial A_m} & \frac{\partial F_m}{\partial B_1} & \cdots & \frac{\partial F_m}{\partial B_m} \\ \frac{\partial G_1}{\partial A_1} & \frac{\partial G_1}{\partial A_2} & \cdots & \frac{\partial G_1}{\partial A_m} & \frac{\partial G_1}{\partial B_1} & \cdots & \frac{\partial G_1}{\partial B_m} \\ \frac{\partial G_2}{\partial A_1} & \frac{\partial G_2}{\partial A_2} & \cdots & \frac{\partial G_2}{\partial A_m} & \frac{\partial G_2}{\partial B_1} & \cdots & \frac{\partial G_2}{\partial B_m} \\ \vdots & \vdots & \ddots & \vdots & \vdots & \ddots & \vdots \\ \frac{\partial G_m}{\partial A_1} & \frac{\partial G_m}{\partial A_2} & \cdots & \frac{\partial G_m}{\partial A_m} & \frac{\partial G_m}{\partial B_1} & \cdots & \frac{\partial G_m}{\partial B_m} \end{pmatrix}$$

The different derivatives are found directly from the differential equations (4.58):

$$\frac{\partial F_i}{\partial A_j} = \begin{cases} -\beta B_i + D_A \left(\frac{ip(j)}{\langle k \rangle} - 1 \right) , & \text{if } i = j, \\ D_A \frac{ip(j)}{\langle k \rangle} , & \text{if } i \neq j. \end{cases}$$

$$\frac{\partial F_i}{\partial B_j} = \begin{cases} \mu - \beta A_i , & \text{if } i = j, \\ 0 , & \text{if } i \neq j. \end{cases}$$

$$\frac{\partial G_i}{\partial A_j} = \begin{cases} \beta B_i , & \text{if } i = j, \\ 0 , & \text{if } i \neq j. \end{cases}$$

$$\frac{\partial G_i}{\partial B_j} = \begin{cases} \beta A_i - \mu + D_B \left(\frac{ip(j)}{\langle k \rangle} - 1 \right) , & \text{if } i = j, \\ D_B \frac{ip(j)}{\langle k \rangle} , & \text{if } i \neq j. \end{cases}$$

We want to examine the stability when $B_i = 0$ and $A_i = \frac{i}{\langle k \rangle}\rho$. Inserting this into the above equations yields

$$\frac{\partial F_i}{\partial A_j} = \begin{cases} D_A \left(\frac{ip(j)}{\langle k \rangle} - 1 \right) , & \text{if } i = j, \\ D_A \frac{ip(j)}{\langle k \rangle} , & \text{if } i \neq j. \end{cases}$$

$$\frac{\partial F_i}{\partial B_j} = \begin{cases} \mu - \beta \frac{i}{\langle k \rangle}\rho , & \text{if } i = j, \\ 0 , & \text{if } i \neq j. \end{cases}$$

$$\frac{\partial G_i}{\partial A_j} = 0 .$$

$$\frac{\partial G_i}{\partial B_j} = \begin{cases} \beta \frac{i}{\langle k \rangle}\rho - \mu + D_B \left(\frac{ip(j)}{\langle k \rangle} - 1 \right) , & \text{if } i = j, \\ D_B \frac{ip(j)}{\langle k \rangle} , & \text{if } i \neq j. \end{cases}$$

Although finding the eigenvalues to this matrix analytically might be difficult, we can calculate them numerically. By varying the particle density ρ, one can determine the point where the largest eigenvalue turns positive, *i.e.* when $\rho = \rho_c$. This result can then be compared to the results given by the series expansion.

Simulation results

In Fig. 4.11 we show our simulation results together with analytical results. Both Colizza's result for $D_{A,\text{disc}} = D_{B,\text{disc}} = 1$ (Eq. (4.20b)), our result with series expansion and the Jacobian matrix are shown. As seen in the figure, a high order series expansion seems to match the Jacobian matrix results very well. We must assume that this agreement is more than just a coincidence, and that a high enough order will be an exact match. Since the two quite different approaches seem to give the same results, we suggest that this is the best result one can get without discarding the mean-field approximation.

We see from the figure that the value of D_A has little impact on the location of the phase transition. The B particle diffusion D_B, however, significantly changes the critical density ρ_c. Interestingly, lower diffusion rate D_B actually *lowers* the critical density ρ_c. This means that a particle density which (with fast diffusion) would not cause a long-term infection, can with slower diffusion actually spread an infection. This is in stark contrast to the common advice of reducing travel to prevent an epidemic or pandemic. In our case, reducing travel (diffusion) can actually contribute to the spreading of the infection. The explanation for this may be that without a fast diffusion, B particles are not transported away from high degree nodes, where they have many A particles to infect, to low degree nodes, where there are fewer A particles.

4.4.2 Type II

From previous results we know that the stationary state for type II reactions is

$$\overline{\rho}_B = \rho\left(1 - \frac{\mu}{\beta}\right),$$

regardless of the value of D_A (but with positive D_B). Thus, there is no phase transition when varying ρ. There is, however, a phase transition when varying μ/β, and the transition occurs when $\mu = \beta$.

4.4.3 Type M

Series expansion

As mentioned earlier, the series expansion for type M is an alternating and diverging one, and therefore of little use, also when locating the phase transition.

Jacobian matrix

As with type I, we can calculate the eigenvalues of the Jacobian matrix to determine where the phase transition occurs. The different derivatives are found directly from the

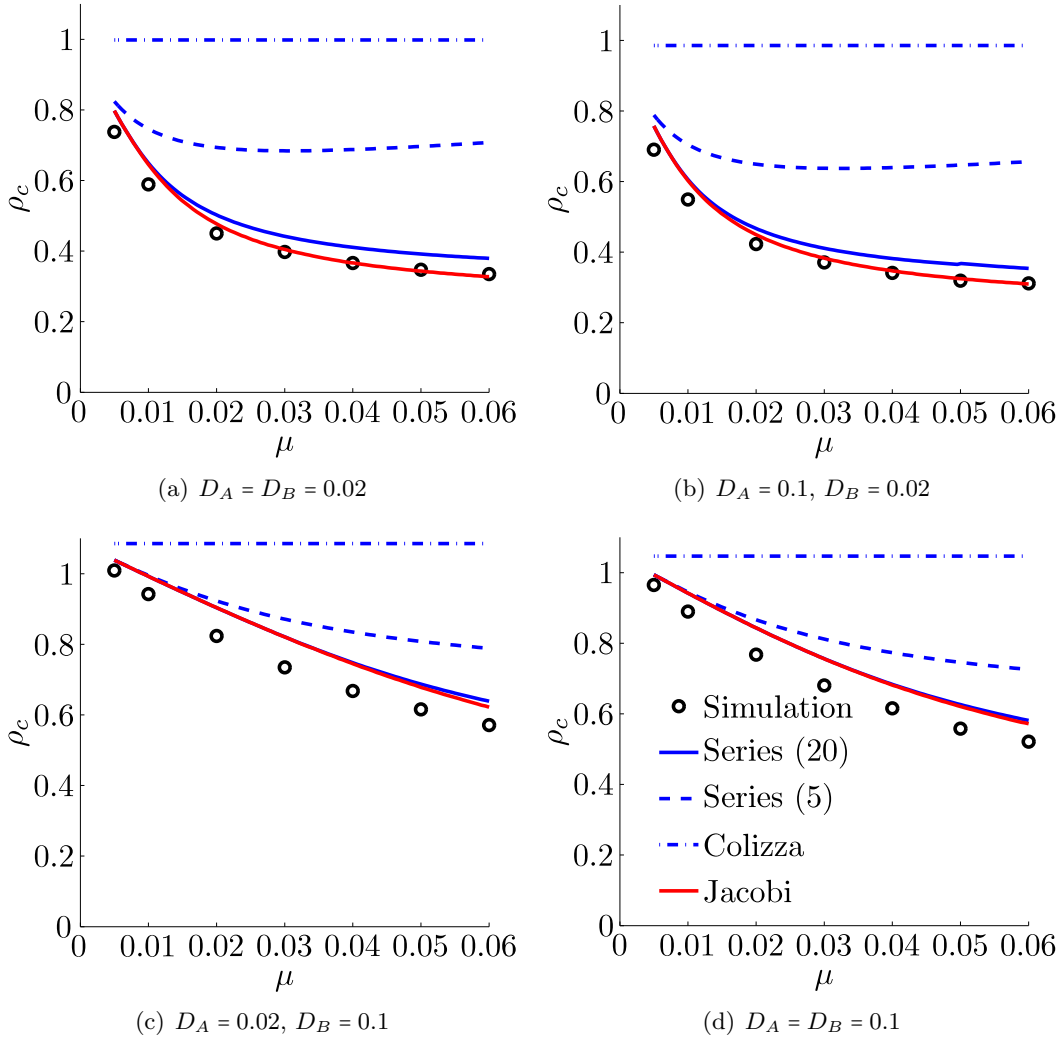

(a) $D_A = D_B = 0.02$

(b) $D_A = 0.1$, $D_B = 0.02$

(c) $D_A = 0.02$, $D_B = 0.1$

(d) $D_A = D_B = 0.1$

Figure 4.11: Location of phase transition for type I reactions, with $\mu/\beta = 2$. The network is scale-free with $V = 1000$ and $\gamma = 2.5$.

differential equations (4.58):

$$\frac{\partial F_i}{\partial A_j} = \begin{cases} -\beta \frac{B_i(\rho_\times + B_i)}{(\rho_\times + A_i + B_i)^2} + D_A \left(\frac{ip(j)}{\langle k \rangle} - 1 \right) , & \text{if } i = j, \\ D_A \frac{ip(j)}{\langle k \rangle} , & \text{if } i \neq j. \end{cases}$$

$$\frac{\partial F_i}{\partial B_j} = \begin{cases} \mu - \beta \frac{A_i(\rho_\times + A_i)}{(\rho_\times + A_i + B_i)^2} , & \text{if } i = j, \\ 0 , & \text{if } i \neq j. \end{cases}$$

$$\frac{\partial G_i}{\partial A_j} = \begin{cases} \beta \frac{B_i(\rho_\times + B_i)}{(\rho_\times + A_i + B_i)^2} , & \text{if } i = j, \\ 0 , & \text{if } i \neq j. \end{cases}$$

$$\frac{\partial G_i}{\partial B_j} = \begin{cases} -\mu + \beta \frac{A_i(\rho_\times + A_i)}{(\rho_\times + A_i + B_i)^2} + D_B \left(\frac{ip(j)}{\langle k \rangle} - 1 \right) , & \text{if } i = j, \\ D_B \frac{ip(j)}{\langle k \rangle} , & \text{if } i \neq j. \end{cases}$$

We want to examine the stability when $B_i = 0$ and $A_i = \frac{i}{\langle k \rangle}\rho$. Inserting this into the above equations yields

$$\frac{\partial F_i}{\partial A_j} = \begin{cases} D_A \left(\frac{ip(j)}{\langle k \rangle} - 1 \right) , & \text{if } i = j, \\ D_A \frac{ip(j)}{\langle k \rangle} , & \text{if } i \neq j. \end{cases}$$

$$\frac{\partial F_i}{\partial B_j} = \begin{cases} \mu - \beta \frac{i\rho}{\langle k \rangle \rho_\times + i\rho} , & \text{if } i = j, \\ 0 , & \text{if } i \neq j. \end{cases}$$

$$\frac{\partial G_i}{\partial A_j} = 0 .$$

$$\frac{\partial G_i}{\partial B_j} = \begin{cases} \beta \frac{i\rho}{\langle k \rangle \rho_\times + i\rho} - \mu + D_B \left(\frac{ip(j)}{\langle k \rangle} - 1 \right) , & \text{if } i = j, \\ D_B \frac{ip(j)}{\langle k \rangle} , & \text{if } i \neq j. \end{cases}$$

We can then calculate the eigenvalues numerically. By varying the particle density ρ, one can determine the point where the largest eigenvalue turns positive, *i.e.* when $\rho = \rho_c$.

Simulation results

In Fig. 4.12 we show our simulation results together with analytical results. We expect the simulation results to coincide with the Jacobian matrix results. For comparison, we also present the analytical result for $D_{A,\text{disc}} = D_{B,\text{disc}} = 1$ ($D_{A,\text{cont}} = D_{B,\text{cont}} = \infty$, Eq. (4.22)), *i.e.* when $\overline{\rho}_{A,k} \sim k$ and $\overline{\rho}_{B,k} \sim k$. We see that the Jacobian matrix approach gives a very good result, close to the simulation results.

The results show many similarities with the type I results. The diffusion rate D_A for A particles has little effect on the critical density, while D_B clearly affects it. Also for type M, lowering the diffusion rate D_B lowers the critical density ρ_c.

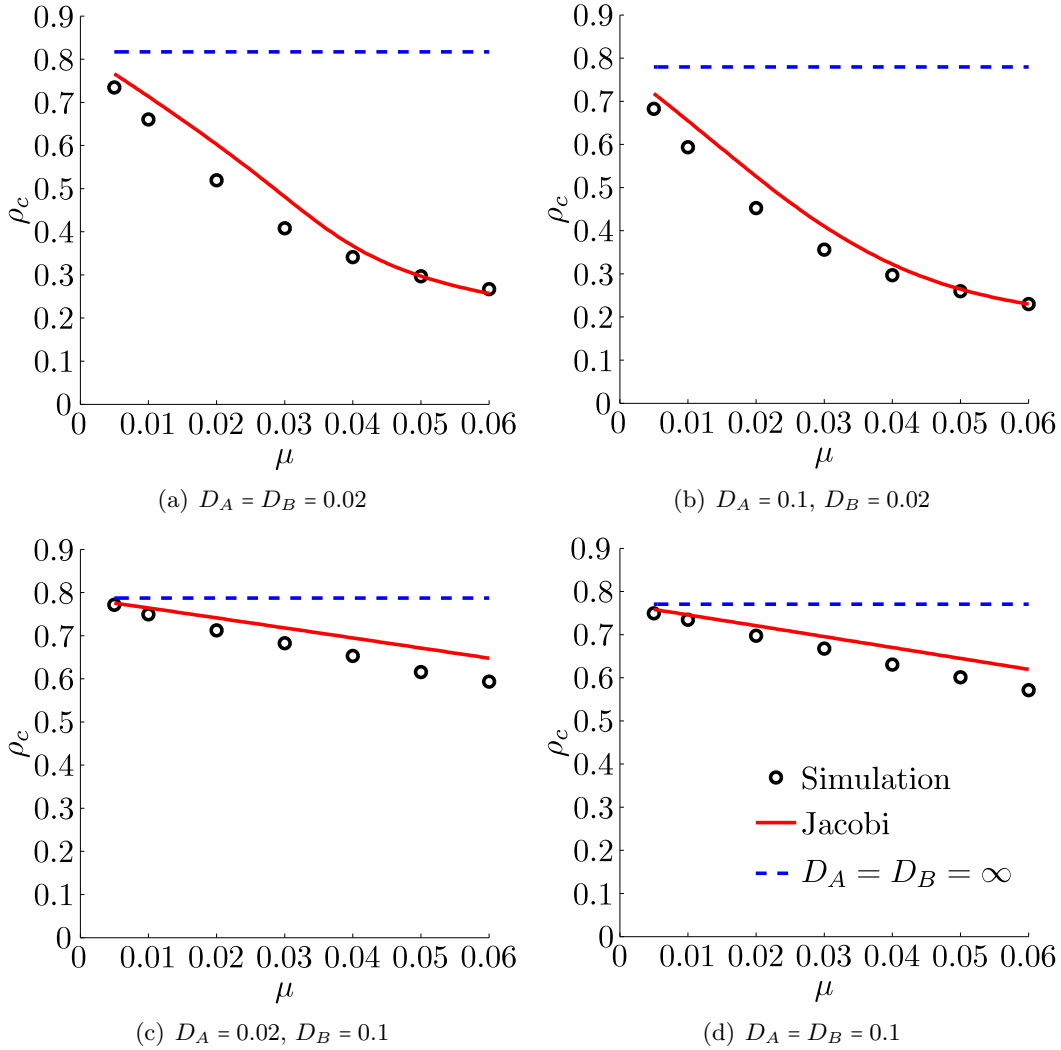

(a) $D_A = D_B = 0.02$

(b) $D_A = 0.1$, $D_B = 0.02$

(c) $D_A = 0.02$, $D_B = 0.1$

(d) $D_A = D_B = 0.1$

Figure 4.12: Location of phase transition for type M reactions, with $\beta/\mu = 2$. Network is scale-free with $V = 1000$ and $\gamma = 2.5$.

Chapter 5

Other reaction-diffusion models

As an example of other applications of reaction-diffusion processes on networks, we will in this chapter present a model for opinion formation. Opinion formation is a field of sociophysics, which uses methods from physics to explain or understand sociological phenomena. One of the early contributions to this field was given by Galam [13]. Later, different models for opinion formation has been presented by Sznajd-Weron and Sznajd [14] and Krapivsky and Redner [15]. The two latter "spin-like" models typically have a long-term limit where all sites have the same opinion (ferromagnetic) or alternating opinions (anti-ferromagnetic). We are therefore interested in creating a new model which has stationary states in which both opinions can coexist (in more complex patterns than the anti-ferromagnetic), which may be more realistic.

We wish to model opinion formation on a network which for example can represent cities or social groups, and connections between them. We let A and B particles represent people with different (binary) opinions A and B, which can persuade each other and move around on the network. To model the travel between cities (or nodes), we let these particles or persons diffuse around on the network. We also associate a *persuasive power* μ with each person, which describes how many persons each person manages to persuade per time step. The process of persuading will be the reaction step in our reaction-diffusion model.

Since every person has the same persuasive power, this results in a variant of *majority rule*. With majority rule, the majority is most likely win an argument, and thus further increase its majority. Many variants of majority rule has been presented, *e.g.* the Sznajd model [14] and MR (Majority Rule) model of Krapivsky and Redner [15]. Both these models represent opinions as spins placed on some kind of lattice, with interactions between neighboring spins. To our knowledge, however, no model has been presented which let the spin particles or persons move around in a network, with interaction only between particles within the same node.

5.1 Master equations

To describe the time evolution of our opinion model, we use master equations similar to those used for the epidemic model presented earlier. Let $N_A(i,t)$ and $N_B(i,t)$ represent

the number of A and B particles, respectively, at node i at time t, as before. The diffusion rates D_A and D_B are the probabilities that A and B particles, respectively, will diffuse in each time step. Together with the persuasive power $\mu > 0$, this leads to the master equations

$$\partial_t N_A(i,t) = \mu\left[N_A(i,t) - N_B(i,t)\right] - D_A N_A(i,t) + D_A \sum_{j\epsilon U(i)} \frac{N_A(j,t)}{k_j}\,, \tag{5.1}$$

$$\partial_t N_B(i,t) = \mu\left[N_B(i,t) - N_A(i,t)\right] - D_B N_B(i,t) + D_B \sum_{j\epsilon U(i)} \frac{N_B(j,t)}{k_j}\,. \tag{5.2}$$

where $U(i)$ denotes the set of neighboring nodes of node i. Here, the terms with μ describes the persuasion of the other opinion, while the two latter terms describes the diffusion of particles away from and into the node, respectively. To make sure all particle numbers are positive, these equations have to be limited when implemented, so that $N_A(i,t) > 0$ and $N_B(i,t) > 0$ [1].

By looking at limiting cases of the master equations (5.2), we can learn something about the stationary state of the system. In the limit $D_A, D_B \to 0$ (no diffusion), we are left with $\partial_t N_A(i,t) = -\partial_t N_B(i,t) = \mu[N_A(i,t) - N_B(i,t)]$. This implies that if $N_A(i,0) > N_B(i,0)$, the node will end up with only A particles. Similar arguments can be used if B particles are initially in the majority. Thus, depending on the inital state, one can have a stationary state with some nodes with A particles in majority and some nodes with B particle majority.

Another limit to investigate, is when the diffusion dominates over the reaction, *i.e.* $D_A, D_B \gg \mu$. In this case, the dominating diffusion makes it possible to consider the whole network as a single node. So if the inital total number of A particles exceeds the number of B particles, $N_A(0) > N_B(0)$, the stationary state will have only A particles.

Between these two limits, we expect there to be a transition between a stationary state just dependent on local properties (first case) to a state only dependent on global properties (second case). To describe this transition, we present simulation results in section 5.2. In our simulations, the master equations (5.2) were implemented with forward difference.

5.2 Simulation results

We performed simulations to investigate the behavior of the model. More specifically, we were interested in how the stationary state depends on μ, D_A and D_B. We let the initial state be a random distribution of A and B particles, but with equal total number of A and B particles ($N_A(t=0) = N_B(t=0)$). The total (conserved) particle number is $N = N_A(t) + N_B(t)$, as before.

In Fig. 5.1, we show results for the fraction N_m/N where N_m is the number of majority particles. We recognize the limits discussed in the previous section. With slow diffusion

[1] One could imagine a more intricate reaction term, *e.g.* $\mu(N_A(i,t) - N_B(i,t))N_A(i,t)N_B(i,t)/N(i,t)^2$, which ensures that $N_A(i,t) > 0$ and $N_B(i,t) > 0$. This will not be considered here.

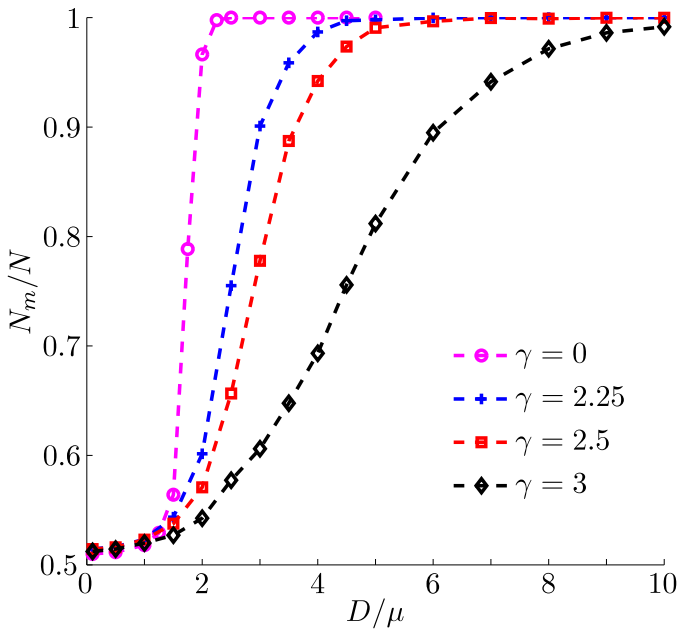

Figure 5.1: Fraction of majority particles in the stationary state, with $D_A = D_B = D$. The results were obtained by averaging over 600 samples (20 networks, 30 simulations per network). The networks were scale-free with $V = 1000$ nodes.

$(D_A, D_B \ll \mu)$, the stationary state of each node is just dependent on its initial state $N_A(i, t = 0)$ and $N_B(i, t = 0)$. Since the particles were randomly distributed initially, there is an (almost) equal number of nodes A and B majority, and thus $N_m/N \approx 1/2$. When diffusion dominates $(D_A, D_B \gg \mu)$, the minority will not survive, and all particles will be majority particles $(N_m = N)$.

Figure 5.1 shows results for scale-free networks with different exponents γ. A low exponent makes it more probable with high degree nodes, while a high exponent gives a network with many low degree nodes and few high degree hubs. We have chosen to show results for $\gamma \in \{2.25, 2.5, 3.0\}$ because real-world networks often have exponents in this area (see *e.g.* [5]). In addition we show results for $\gamma = 0$, to illustrate how the model behaves in a very dense network. When $\gamma = 0$, all degrees are equally probable, and hence the network is very densely connected.

We see from figure 5.1 that network topology has a huge impact on the fraction of majority nodes. For $\gamma = 3$, significantly stronger diffusion is needed to distribute the majority opinion to the whole network, than for $\gamma < 3$. This is because higher γ causes a less closely connected network, with few high degree nodes. For a more densely connected network $(\gamma = 0)$, there seems to be a sudden change at $D_A \approx 2\mu$ where the minority opinion suddenly disappears.

The results in figure 5.1 indicate that an opinion spreads more easily in a closely connected network. This is perhaps not surprising, since a closely connected network

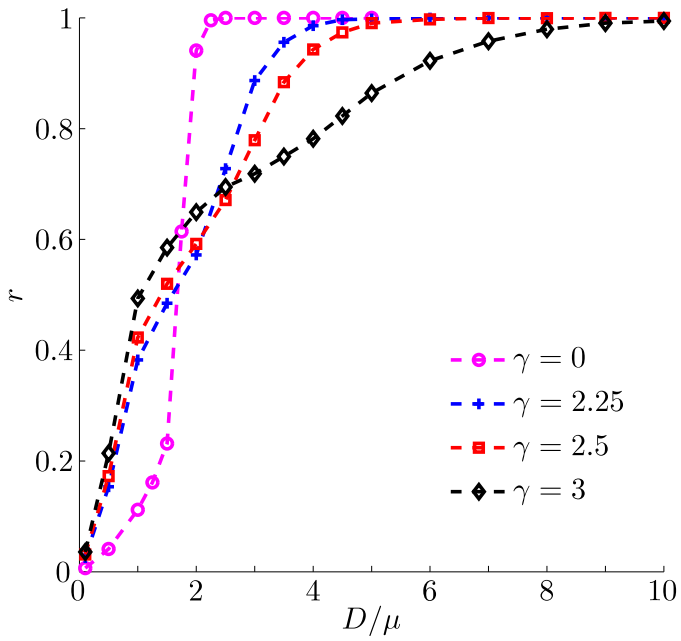

Figure 5.2: Fraction r of links connecting same-spin nodes in the stationary state, with $D_A = D_B = D$. The results were obtained by averaging over 600 samples (20 networks, 30 simulations per network). The networks were scale-free with $V = 1000$ nodes.

causes more communication between different opinions, thus increasing the chance of being persuaded by the majority.

Next, we will try to look at the relation between which particles are in majority at neighboring nodes. First, to simplify the terminology, we introduce a spin quantity to describe which particle type is in majority. The spin $\sigma(i,t)$ of a node i at time t is defined as

$$\sigma(i,t) = \begin{cases} 1\,, & \text{if } N_A(i,t) \geq N_B(i,t), \\ -1\,, & \text{if } N_B(i,t) < N_A(i,t). \end{cases} \tag{5.3}$$

Thus, if two neighbor nodes i and j have the same particle type in majority, $\sigma(i,t)\sigma(j,t) = 1$, and otherwise $\sigma(i,t)\sigma(j,t) = -1$. Using this spin quantity, we can easily calculate the correlation r between neighboring nodes' spin:

$$r(t) = \frac{1}{2V\langle k\rangle} \sum_{i=1}^{V} \sigma(i,t) \sum_{j \in U(i)} \sigma(j,t)\,. \tag{5.4}$$

We recall that V is the number of nodes in the network, and $U(i)$ is the set of neighboring nodes of node i. Since there are $V\langle k\rangle$ links and every link is counted twice, the normalization factor is $1/(2V\langle k\rangle)$.

Figure 5.2 shows the correlation r in the stationary state as function of D/μ ($D_A = D_B = D$). As one would expect, there is no correlation when diffusion is negligible, since

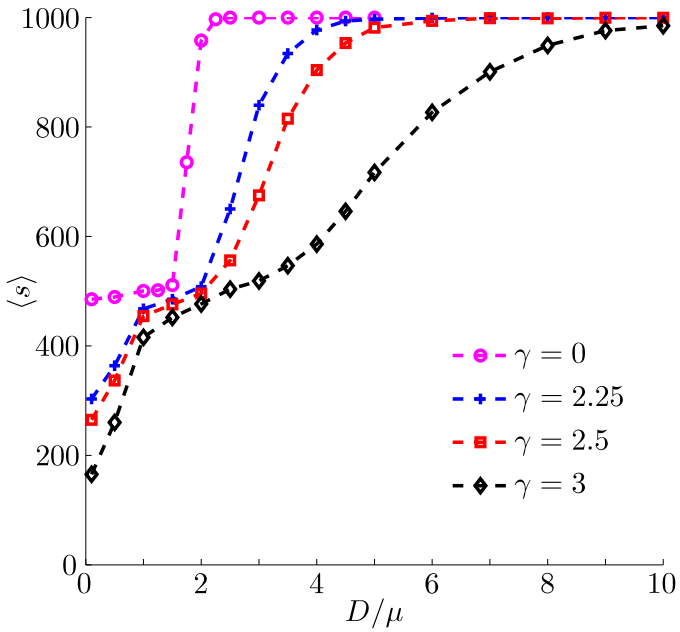

Figure 5.3: Average clique size in the stationary state for a randomly chosen node. The diffusion constant was $D_A = D_B = D$. The results were obtained by averaging over 600 samples (20 networks, 30 simulations per network). The networks were scale-free with $V = 1000$ nodes.

the nodes then practically will be independent of other nodes. When diffusion is strong, however, all nodes will eventually have the same spin (or opinion), and thus the correlation is $r = 1$. The interesting part of this figure lies in the transition between these two limits.

We can see that for diffusion rates on the same order as reaction rates, $D \sim \mu$, the networks with $\gamma = 3$ actually have a larger neighbor correlation than the other networks. When comparing with Fig. 5.1, we see that when $D/\mu = 2$, no significant majority has formed yet (for $\gamma = 3$). However, at this point, the neighbor correlation r is quite strong, with $r \approx 0.65$. The correlation is far stronger than for $\gamma = 2.25$, which has a significantly larger majority for $D/\mu = 2$.

That there is no clear majority but significant correlation, must mean that there are many small clusters or "cliques" with same-spin nodes. However, with slow diffusion, the networks are too loosely connected to be able to convert neighboring "cliques". The network topology makes it necessary with faster diffusion to achieve a spreading of the majority opinion.

It would be interesting to look at how the clique sizes $\{S_i\}$ evolve with increasing diffusion. Let C be the total number of cliques, S_i be the size of clique i and s_i the size of the clique which contains node i. "Average clique size" can then be interpreted in (at least) two ways: $\langle S \rangle$ or $\langle s \rangle$. The first interpretation is just the average size of all cliques,

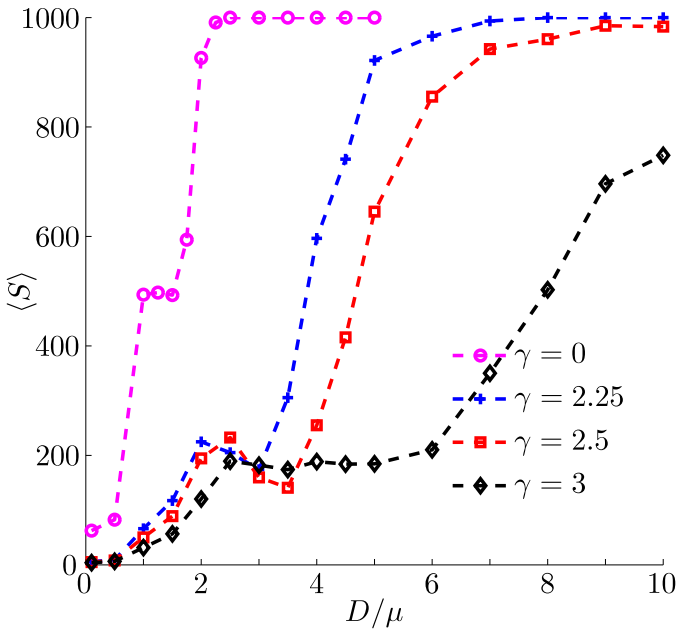

Figure 5.4: Average clique size in stationary state. The diffusion constant was $D_A = D_B = D$. The results were obtained by averaging over 600 samples (20 networks, 30 simulations per network). The networks were scale-free with $V = 1000$ nodes.

i.e.

$$\langle S \rangle = \frac{1}{C} \sum_{i=1}^{C} S_i \ .$$

The other interpretation corresponds to the average clique size when choosing a random node,

$$\langle s \rangle = \frac{1}{V} \sum_{i=1}^{V} s_i \ .$$

Since each clique i contributes with S_i nodes, each with a clique size S_i, we get the following relation between $\langle s \rangle$ and $\langle S^2 \rangle$:

$$\langle s \rangle = \frac{1}{V} \sum_{i=1}^{C} S_i^2 = \frac{C}{V} \langle S^2 \rangle \ .$$

In figure 5.3 we show simulation results which show how the clique sizes evolves as the diffusion rate increases. We see that a higher γ gives smaller cliques. Due to the sparse connections for $\gamma = 3$, small cliques of nodes are sufficient to increase the neighbor correlation r significantly, with only few connections between the cliques. With lower γ, larger cliques are necessary to achieve the same correlation, because these networks are more densely connected.

To find out more about the clique size distribution, we also present results for the average clique size $\langle S \rangle$ (in Fig. 5.4) and the largest clique size $\max(S)$ (in Fig. 5.5). We

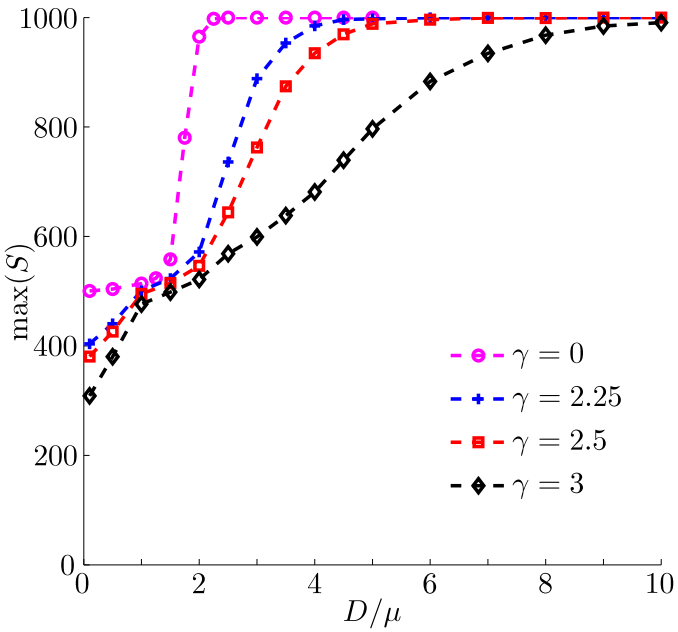

Figure 5.5: Maximum clique size in the stationary state. The diffusion constant was $D_A = D_B = D$. The results were obtained by averaging over 600 samples (20 networks, 30 simulations per network). The networks were scale-free with $V = 1000$ nodes.

see that the average clique size $\langle S \rangle$ for $\gamma \in \{2.25, 2.5, 3\}$ actually *decreases* in the region around $D \approx 3\mu$. In this region, both the average node clique size $\langle s \rangle$ and the maximum clique size increases. The only explanation for this must be that there are a number of medium sized clusters around $D \approx 2\mu$. When increasing D, these clusters split, which increases both the number of small clusters and the size of the largest cluster. This decrease in $\langle s \rangle$ must be said to be quite peculiar. One could suspect that it is caused by stochastic variations, but each data point in these figures is the result of 600 separate simulations, so that should not be the case. The reason for this "dip" should be investigated further.

All in all, if one interprets this in a social context with cities as nodes, we can conclude that more travel (diffusion) gives more homogeneous opinions. This seems to make sense, since communication (obviously) is necessary for spreading information or opinions. We can also see that the way cities or countries are connected, matters a great deal for how easily opinion spreads between them, as a network with many hubs (low γ) is more efficient at spreading an opinion. We have also learned that with quite low diffusion, long before one opinion has gained significant majority, there is a high correlation between the opinion of neighbor cities. In other words, clusters of same-opinion cities form, eventually followed by the merging of these clusters, and finally a homogeneous opinion forms throughout the network.

Until now, we have let the A and B particles diffuse with the same rate, $D_A = D_B = D$. One could, however, imagine that different opinions lead to different travel patterns, and

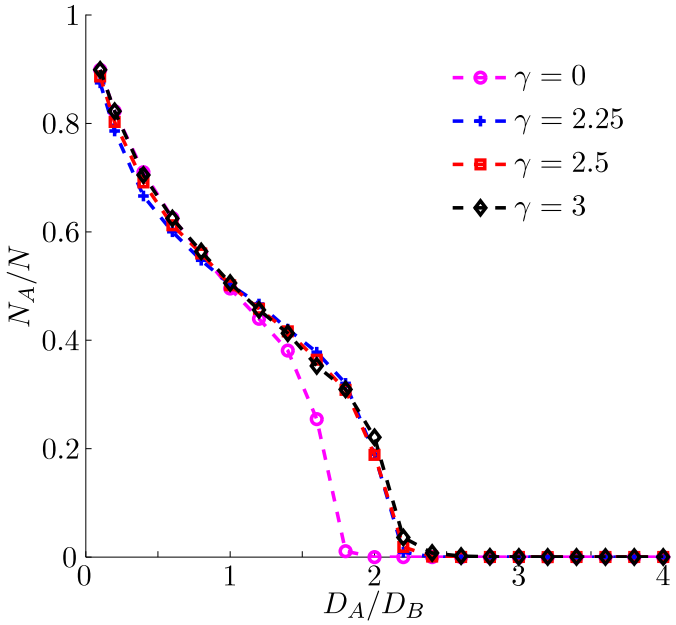

Figure 5.6: Fraction of A particles in the stationary state, with $D_B = \mu$. The results were obtained by averaging over 100 samples (10 networks, 10 simulations per network). The networks were scale-free with $V = 1000$ nodes.

thus different diffusion constants. We will therefore investigate how the stationary state behaves when $D_B = \mu$ and varying D_A.

Figure 5.6 shows the fraction of A particles in the stationary state. Surprisingly, increasing the diffusion constant D_A actually *decreases* the number of A particles. This is quite contra-intuitive, as we found previously that increasing diffusion ($D = D_A = D_B$) is necessary for spreading a majority opinion to the whole network.

One explanation for this behavior can be that less diffusion makes to easier to keep the majority nodes that a particle type already has conquered. As mentioned earlier, initially the A and B particles are distributed randomly. One can imagine that in the first stage of the process, the majority of each node (almost) eliminates the minority. In the next stage, the quick diffusing A particles diffuse into B majority nodes, in which they are absorbed. The B particles, however, mostly stay in place. After a while, the nodes are emptied for A particles, and the B particles can slowly diffuse into and conquer them.

In figures 5.7, 5.8 and 5.9 we show how the clique sizes evolve as function of D_A/D_B. We see that there is fairly little change (at least for $\gamma \in \{2.25, 2.5, 3.0\}$) from $D_A \ll D_B$ to $D_A = 2D_B$. At $D_A = 2D_B$ there is a sudden jump where the cliques merge to form a single clique. One could say that there is a condensation or phase-transition at $D_A = 2D_B$, where the whole network is occupied by B particles.

The behavior of $\gamma = 0$ is slightly different, although it also shows the same sudden jump in $\langle s \rangle$ and $\max(S)$. Since the nodes in this network are so closely connected, any node can be reached in very few steps from any other. Therefore, almost all A nodes belong

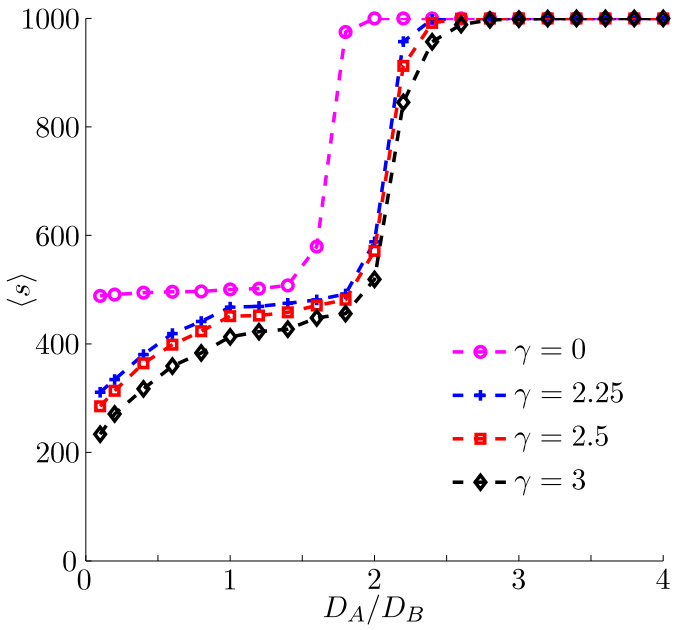

Figure 5.7: Average clique size in the stationary state for a randomly chosen node. The B diffusion constant was $D_B = \mu$. The results were obtained by averaging over 100 samples (10 networks, 10 simulations per network). The networks were scale-free with $V = 1000$ nodes.

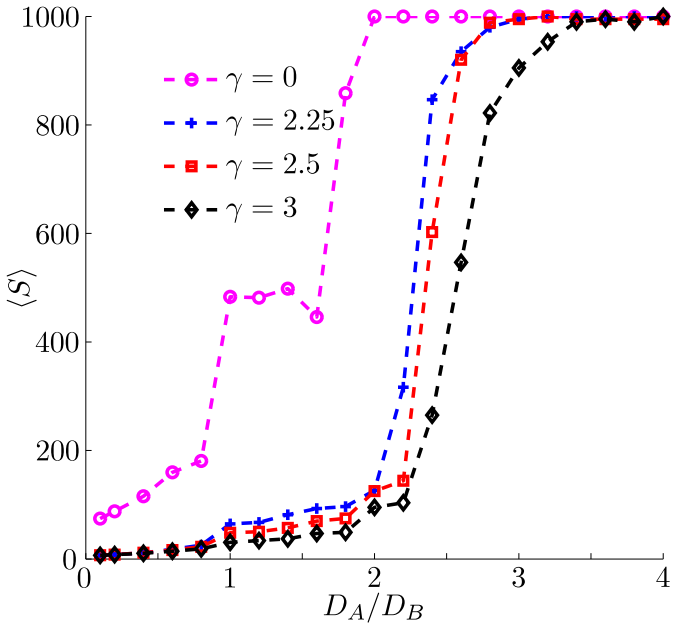

Figure 5.8: Average clique size in the stationary state. The B diffusion constant was $D_B = \mu$. The results were obtained by averaging over 100 samples (10 networks, 10 simulations per network). The networks were scale-free with $V = 1000$ nodes.

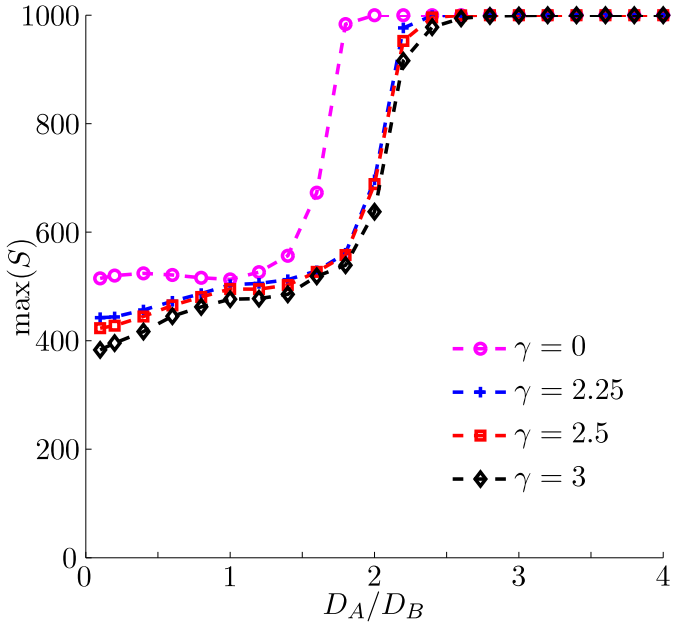

Figure 5.9: Maximum clique size in the stationary state. The B diffusion constant was $D_B = \mu$. The results were obtained by averaging over 100 samples (10 networks, 10 simulations per network). The networks were scale-free with $V = 1000$ nodes.

to the same cluster, and thus $\langle s \rangle \approx 500$ (when $D_A < 2D_B$). The results for $\langle S \rangle$, however, show that there still exists small clusters not connected to the main cluster for $D_A < D_B$. Not until $D_A = D_B$ does the average cluster size $\langle S \rangle$ increase to ≈ 500, where all nodes belong to the large cluster.

The results for the case where $D_A \neq D_B$ show that the behavior of this model is far from simple or obvious. In a social context, this last result means that *less* travel actually could be beneficial to spread one's opinion. By staying together, one will convert people with other opinions traveling into a city, and then slowly migrate when the neighbor cities are almost emptied for other opinions.

We have shown that this model is seemingly more complex than one would initally think. Although the model already shows complex behavior, we can readily think of changes to adapt it to more realistic cases. An interesting extension of the model would be to include more than two (binary) opinions. One could theoretically have infinitely many opinions described in the same way we have done with the two A and B opinions. It would also be interesting to investigate a model with different persuasive power μ for different opinions. Finally, one could model the persuasion process differently with another reaction term in the master equations, which in itself ensure that $N_A(i,t) > 0$ and $N_B(i,t) > 0$.

Chapter 6

Conclusion and outlook

We have considered a reaction-diffusion process on complex networks. In particular, we have studied the so-called susceptible-infected-susceptible (SIS) model on networks. This model describes the behavior of an infection where one has two types of particles: susceptible and infected. A simple reaction model governing the infection by susceptible particles and the recovery of infected particles is used. A diffusion process distributes these particles around on the network.

Within the SIS model, we have studied the long-term behavior (stationary state) with different networks and parameters. Previously, the stationary state was studied by Colizza, Pastor-Satorras and Vespignani [8]. These authors present both analytical and simulation results for this state and demonstrate that there exists a phase transition at a critical density. Below this density there are no infected particles in the stationary state, and above it, an infection will always persist. Previous work [2] reviewed and reproduced their analytic (mean-field) results, but also reveiled that their simulations deviate from the analytical expressions. This applied both to the location of the phase transition as well as the quantitative behavior. The simulations in Ref. [2], however, matched the analytical expressions accurately. In this thesis, we have put forward a plausible explanation for the deviation between simulation and analytical results in Ref. [8]. This was demonstrated by implementing the reaction-diffusion process as done in Ref. [8] and then performing simulations with excessively high reaction rates. Too high reaction rates lead to a saturation of the reaction (giving a reaction probability greater than one), which alters the stationary state.

We have also presented an analytical approach based on continuous time (as proposed by Saldaña [10]), whereas the approach of Colizza *et al.* [8] was based on discrete time. The differences and similarities between these two approaches were discussed. We continued with finding analytical solutions for all values of the diffusion constants by a series expansion in the degree k. We also presented analytical results for a new reaction type (in addition to two reaction types proposed in Ref. [8]) which was meant to better resemble a real-life situation. Simulation results match well with the analytical (mean-field) series solution for parameters where the mean-field approximation is a good approximation. Finally, we presented analytical and simulation results for the critical density, at which

the phase transition occurs. Both a series expansion and a Jacobian matrix was used to predict this density, and simulation results agree well with these analytical results.

As an example of other uses of reaction-diffusion processes on networks, a model for opinion formation and spreading was proposed. This model was meant to resemble the complexity of the real world in a better way than existing models. Simulation results show that the model has some interesting and unexpected behavior. Further work on this model can reveal more on how the opinion spreads and how clusters of same-opinion nodes form. Expanding the model to include more than two opinions would also be interesting.

Bibliography

[1] M. M. Waldrop. *Complexity: The Emerging Science at the Edge of Order and Chaos.* Simon and Chuster, New York, 1992.

[2] Halvor Lund. Epidemic modeling on complex networks. *Project thesis, Department of Physics, NTNU*, 2008.

[3] P. Erdös and A. Rényi. On random graphs. *Publ. Math. Debrecen*, 6:290–297, 1959.

[4] Reka Albert and Albert-Laszlo Barabási. Statistical mechanics of complex networks. *Reviews of Modern Physics*, 74:47, 2002.

[5] M. E. J. Newman. The structure and function of complex networks. *SIAM Review*, 45:167–256, 2003.

[6] Q. Chen, H. Chang, R. Govindan, S. Jamin, S. J. Shenker, and W. Willinger. The origin of power laws in internet topoligies revisited. *Proceedings of the 21st Annual Joint Conference of the IEEE Computer and Communications Societies, IEEE Computer Society, Los Alamitos, CA*, 2002.

[7] S. Redner. How popular is your paper? An empirical study of the citation distribution. *Eur. Phys. J. B*, 4:131–134, 1998.

[8] Vittoria Colizza, Romualdo Pastor-Satorras, and Alessandro Vespignani. Reaction-diffusion processes and epidemic metapopulation models in complex networks. *Nature Physics*, 3:276–282, Mar 2007.

[9] M. Molloy and B. Reed. A critical point for random graphs with a given degree sequence. *Random Structures and Algorithms*, 6:161–180, 1995.

[10] Joan Saldaña. Continuous-time formulation of reaction-diffusion processes on heterogeneous metapopulations. *Physical Review E*, 78, 2008.

[11] Ingve Simonsen. Diffusion and networks: A powerful combination! *Physica A*, 357:317–330, 2005.

[12] M. E. J. Newman, S. H. Strogatz, and D. J. Watts. Random graphs with arbitrary degree distributions and their applications. *Phys. Rev. E*, 64(2):026118, Jul 2001.

[13] Serge Galam. Social paradoxes of majority rule voting and renormalization group. *Journal of Statistical Physics*, 61(3/4), 1990.

[14] Katarzyna Sznajd-Weron and Józef Sznajd. Opinion evolution in closed community. *Int. Jour. Mod. Phys. C*, 11(6):1157–1165, 2000.

[15] P. L. Krapivsky and S. Redner. Dynamics of majority rule in two-state interacting spin systems. *Phys. Rev. Lett.*, 90(23):238701, Jun 2003.